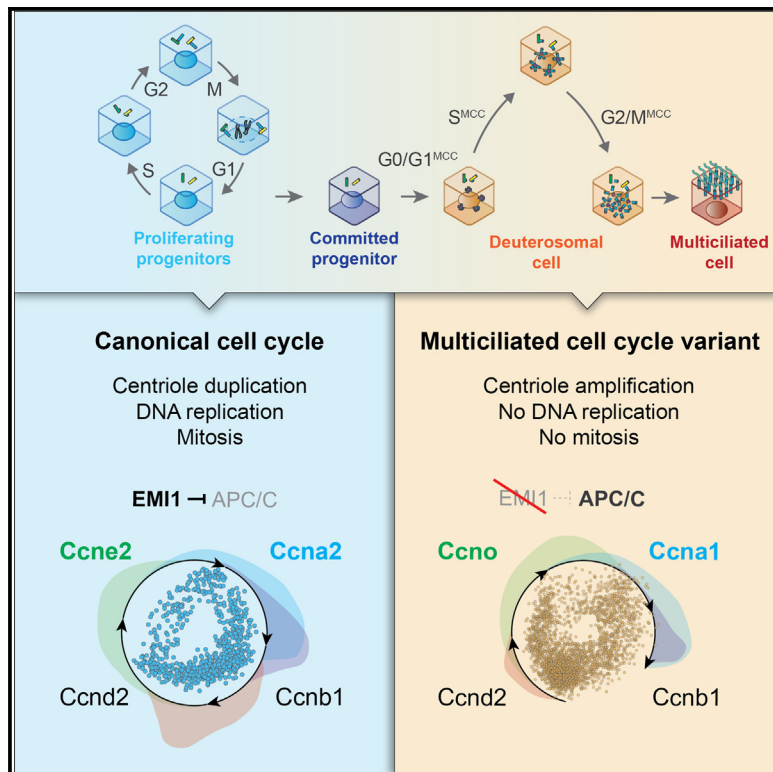


Cyclin switch tailors a cell cycle variant to orchestrate multiciliogenesis

Graphical abstract



Authors

Jacques Serizay, Michella Khouri Damaa, Amélie-Rose Boudjema, ..., Nathalie Spassky, Romain Koszul, Alice Meunier

Correspondence

jacques.serizay@pasteur.fr (J.S.), alice.meunier@bio.ens.psl.eu (A.M.)

In brief

Does a genuine cell cycle variant control centriole amplification in multiciliated cells? Serizay et al. tackle this question by performing single-cell RNA-seq during MCC differentiation. They show that differentiating MCCs co-opt the cell cycle transcriptional topology but switch cyclins and APC/C regulators to divert CDK activity toward differentiation.

Highlights

- A cell cycle variant orchestrates the differentiation of post-mitotic multiciliated cells
- The transcription of most cell cycle factors is reactivated during this cell cycle variant
- Cyclins O and A1 replace the canonical cyclins E2 and A2 in this variant
- Re-expressing *Emi1* or canonical cyclins can reroute differentiation toward the cell cycle



Article

Cyclin switch tailors a cell cycle variant to orchestrate multiciliogenesis

Jacques Serizay,^{1,2,*} Michella Khoury Damaa,¹ Amélie-Rose Boudjema,¹ Rémi Balagué,¹ Marion Faucourt,¹ Nathalie Delgehyr,¹ Laure-Emmanuelle Zaragozi,³ Pascal Barbry,³ Nathalie Spassky,¹ Romain Koszul,² and Alice Meunier^{1,4,*}

¹Institut de Biologie de l'ENS (IBENS), CNRS, INSERM, École Normale Supérieure, PSL Research University, Paris, France

²Institut Pasteur, CNRS UMR3525, Université Paris Cité, Unité Régulation Spatiale des Génomes, Paris, France

³Université Côte d'Azur, CNRS, Institut de Pharmacologie Moléculaire et Cellulaire, 06560 Sophia Antipolis, France

⁴Lead contact

*Correspondence: jacques.serizay@pasteur.fr (J.S.), alice.meunier@bio.ens.psl.eu (A.M.)

<https://doi.org/10.1016/j.celrep.2024.115103>

SUMMARY

Meiosis, endoreplication, and asynthetic fissions are variations of the canonical cell cycle where either replication or mitotic divisions are muted. Here, we identify a cell cycle variant conserved across organs and mammals, where both replication and mitosis are muted, and that orchestrates the differentiation of post-mitotic progenitors into multiciliated cells (MCCs). MCC progenitors reactivate most of the cell cycle transcriptional program but replace the temporal expression of cyclins E2 and A2 with non-canonical cyclins O and A1. In addition, the primary APC/C inhibitor *Emi1* is silenced. Re-expressing cyclins E2 and A2 and/or *Emi1* can induce partial replication or mitosis. This shows that a cell can co-opt the cell cycle genetic program and regulate only certain elements to qualitatively and quantitatively divert CDK activity toward differentiation rather than division. We propose this cell cycle variant to exploit the existence of a cytoplasmic—or centriolar—CDK threshold lower than the S-phase threshold.

INTRODUCTION

Shared factors regulate centriole and DNA duplication processes throughout the cell cycle, and centriole over-duplication is typically associated with genomic instability, accelerating tumor formation and increasing tumor invasiveness (review in Nigg and Holland¹). Centrioles are also the essential component of basal bodies, which act as anchors from which cilia nucleate. Multiciliated cells (MCCs) harbor hundreds of cilia to transport fluids along organ lumens and promote essential respiratory, reproductive, and brain functions. To sustain basal body production required to form hundreds of cilia, post-mitotic MCC progenitors must uncouple centriole biogenesis from cell division to amplify centrioles massively. In the mouse brain, this occurs following three stereotypical phases: the centriole amplification phase, in which centrioles are massively amplifying around “deuterosome” organelles; the centriole growth phase, in which centrioles grow; and finally, the centriole disengagement phase, in which the newly formed centrioles will migrate and dock to the apical plasma membrane to act as a molecular anchor for the future cilia.²

Despite major differences with centriole duplication, such as the absence of DNA replication, mitosis, and cell division, the massive production of centrioles and the intervention of MCC-specific organelles, we and others have previously shown that the activity of individual cell cycle key players, such as MYB, cyclin-dependent kinases CDK2, CDK1,

PLK1, and the APC/C, was essential for accurate control of centriole amplification in MCCs.^{3–8} Pharmacological modulation of the activity of these cell cycle factors induces significant defects in the number of generated centrioles, in the dynamics of their formation, and in motile ciliation in terminally differentiated MCCs and can also induce mitosis-like features and abnormal DNA replication.^{3,5} Here, we use single-cell RNA sequencing (scRNA-seq) profiling to determine whether MCCs co-opt the same type of transcriptional regulation as cycling cells and assess the extent of cell cycle factor expansion. We reveal that MCC differentiation is a genuine variation of the cell cycle. It co-opts more than 70% of cell cycle factors and shares all the features of transcriptional regulation recently characterized in cycling cells. In this variant, CCNO and CCNA1, non-canonical cyclins associated with the expression of genes involved in centriole amplification and motile ciliation, respectively, replace CCNE2 and CCNA2 cyclins canonically engaged in DNA synthesis and mitotic division. We show that a limited expression of canonical cyclins or the *Emi1* APC/C inhibitor further tailors this cell cycle variant. Rescuing the expression of canonical cyclins and/or *Emi1* is sufficient to re-route some differentiating nuclei into partial DNA replication and/or mitotic division. This study shows that MCC differentiation co-opts the optimal principles of gene regulation of the cell cycle and finely tailors the gene set to tune CDK activity and drive an exclusive cytoplasmic process. In a companion study, we further show that *Ccno*, mutated in patients with severe



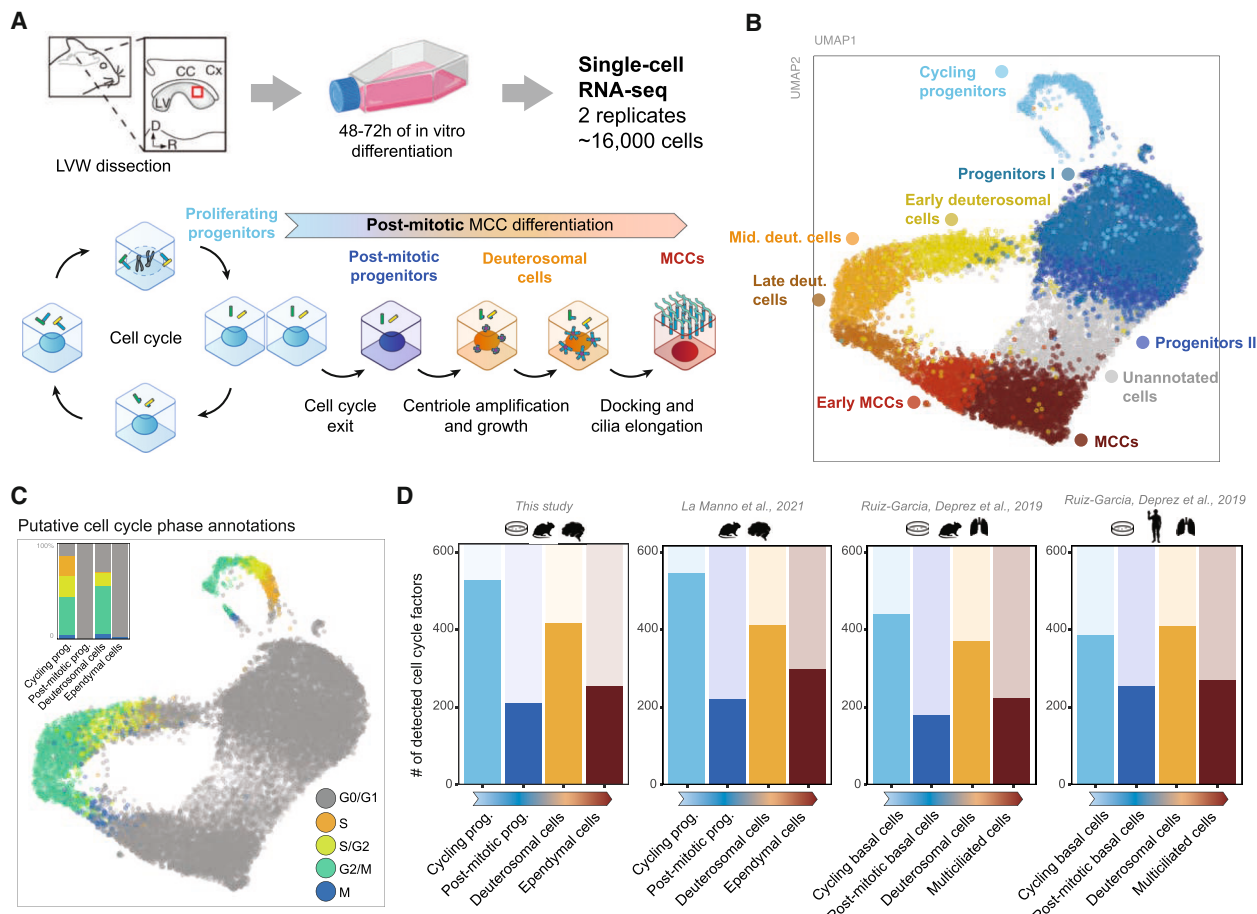


Figure 1. Deuterosomal cells massively co-opt cell cycle factors during post-mitotic differentiation

(A) Single-cell RNA sequencing (RNA-seq) profiling of *in vitro* mouse radial glial cells differentiating into MCCs.
 (B) Uniform manifold approximation and projection (UMAP) of the single-cell RNA-seq dataset. Colors represent annotated cell populations. Post-mitotic progenitor cells, deuterosomal cells, and MCCs have been further divided into smaller cell clusters.
 (C) Putative cell cycle phase annotations inferred using SingleR using neural stem cell reference.¹¹ The inset represents the proportion of each putative cell cycle phase in each cluster.
 (D) Number of cell-cycle-related factors detected in cycling progenitors, post-mitotic progenitors, deuterosomal cells, and MCCs. Single-cell RNA-seq experiments performed *in vitro* or *in vivo* from mouse and human brain or tracheal samples^{12,13} all reveal expression of a large number of cell-cycle-related factors in deuterosomal cells. Cell cycle factors were retrieved from Giotti et al.¹⁴
 See also Figures S1–S3 and Table S1.

congenital ciliopathy, is required to enter this cell cycle variant.⁹ In a study parallel to this work, a different aspect of this cell cycle variant is explored. It shows that another non-canonical player, the transcription factor E2F7, is expressed during respiratory MCC differentiation and involved in securing the DNA replication block and accurate centriole production.¹⁰

RESULTS

Post-mitotic differentiating MCCs massively express cell cycle factors during differentiation

We sought to investigate the extent to which cell cycle factors are co-opted in MCC differentiation. We harvested MCC progenitor cells from lateral ventricle walls of postnatal day (P)1 mouse brains and cultured cycling progenitors to confluence before

inducing their differentiation into MCCs (see STAR Methods). We then profiled the single-cell transcriptomes of 16,401 cells comprising radial glial progenitors during and after they exit the proliferation phase, differentiating MCC progenitors (also known as deuterosomal cells) and terminally differentiated MCCs (Figures 1A and S1A). After removing contaminating cells (e.g., oligodendrocytes, neuroblasts, fibroblasts) and correcting for batch effects (Figure S1B), we annotated four well-defined cell populations subdivided into eight clusters: cycling progenitors (expressing *Mki67*), post-mitotic progenitors (2 clusters marked by *Id1* and *Id3* expression but no *Mki67*), deuterosomal cells (3 clusters: “early,” marked by *Deup1* and *Ccno*; “mid,” marked by max *Deup1* expression; and “late,” marked by *Deup1* and *Ube2c*, deuterosomal cells) and MCCs (2 clusters: “early,” marked by *Ccna1* expression but no *Ube2c*, and

“terminal,” marked by *Tmem212*, MCCs) (Figures 1B and S1C; Table S1; see STAR Methods). The remaining 2,534 unannotated cells showed no clear overexpression of marker genes and were characterized by low clustering stability (Figures S1D and S1E).

Using cell cycle phase transcriptional signatures from a neural stem cell scRNA-seq reference,¹¹ we annotated putative cell cycle phases for each cell. Interestingly, we found that most cells in the deuterosomal population were annotated in the S, G2, or M phase (70% overall), especially in the later deuterosomal sub-cluster (95% of cells annotated in the S, G2, or M phase) (Figures 1C, S1F, and S1G). We leveraged a list of manually curated cell-cycle-related genes ($n = 623$ mouse genes)¹⁴ to investigate their co-option during differentiation. Whereas 85% (527/623) of the cell cycle genes are expressed in cycling progenitors, only 34% (210/623) remained expressed in post-mitotic progenitors (Figure 1D). These numbers are comparable to those observed between proliferating oligodendrocyte progenitors (OPCs) and post-mitotic oligodendrocytes (Figure S1H). However, as much as 67% (417/623) of the cell cycle genes were also expressed in deuterosomal cells. In comparison, only 41% (253/623) remained expressed in post-mitotic MCCs (Figure 1D). This highlights that hundreds of cell cycle genes are reactivated during MCC differentiation, specifically at the deuterosomal stage, during which centrioles are amplifying. We observed a comparable distribution of cell cycle phase transcriptional signatures and a reactivation of cell cycle factors in deuterosomal cells profiled from *in vivo* mouse embryonic brain development¹² as well as from respiratory cells in mouse and human¹³ (Figures 1D and S2), showing that this is not specific to brain MCCs, as recently confirmed by another study,¹⁰ or cultured mouse MCCs and that it is conserved in humans. We validated this observation using a cluster-independent differentiation trajectory analysis (Figure S3). Altogether, these results reveal an unexpected and massive co-option of cell cycle genes during MCC differentiation, across species and tissues, resulting in transcriptional signatures of deuterosomal cells similar to those of cycling cells in different cell cycle phases.

Factors from most cell-cycle-related molecular functions are expressed in deuterosomal cells

Next, we aimed to determine which cell cycle subprocesses the genes re-expressed in deuterosomal cells were explicitly involved. Using the cell cycle factor classification from Giotti et al.,¹⁴ we observed that genes expressed in deuterosomal cells are significantly enriched among 15 of 17 cell-cycle-related sets of genes (Figures 2A and 2B). As expected, nearly all genes related to centrosome regulation (94%, 32/34) are strongly detected in deuterosomal cells (Figure S4A). Interestingly, factors involved in all the other cell-cycle-related processes are also widely co-opted (e.g., all of the 19 genes involved in cytokinesis, 15 out of 19 genes involved in nuclear envelope regulation, etc.) (Figure S4A), suggesting that beyond centriole biogenesis, all cellular compartments may be affected by cell-cycle-like reorganization during MCC differentiation. Notably, 59% of the genes directly involved in DNA replication (30/51) are unexpectedly re-expressed in deuterosomal cells, including several core components of the pre-replication complex (e.g., *Orc2*, *Orc3*, *Orc5*, *Cdt1*), the DNA helicase (e.g., *Mcm3*, *Mcm5*, *Mcm7*), the replisome (*Gins2*, *Gins4*),

all the subunits of the replication factor C complex (*Rfc1–5*), and the catalytic and regulatory subunits of the DNA polymerase alpha (*Pola1* and *Pola2*) (Figure S4A). However, some core members of the pre-replication complex and replisome (*Cdc6*, *Cdc7*, and *Cdc45*) or subunits of the DNA helicase (*Mcm2*, *Mcm5*, *Mcm6*, *Mcm10*) are not detected. This can be explained by findings published during the submission of our manuscript, showing that the expression of the transcription factor E2F7 in respiratory MCCs downregulates the expression of genes involved in DNA replication.¹⁰ Finally, a majority of cell cycle factors involved in DNA condensation, chromosome partition, and kinetochore formation (8/11, 19/26, and 22/25, respectively; Figure S4A), like condensin subunits (e.g., *Smc2*, *Smc4*, *Ncap* proteins, etc.), topoisomerase 2A (*Top2a*, or *CenpA*, are unexpectedly re-expressed in deuterosomal cells. Such recruitment of nuclear factors that apparently have no reason to be expressed in MCCs suggests the existence of cell-cycle-like events in the nucleus during differentiation and/or may indicate unknown functions of these factors in the cytoplasm.

Because we previously showed that an attenuated activity of the mitotic oscillator (CDK1 and APC/C) itself was required during MCC differentiation,³ we compared gene expression of the mitotic oscillator components and their direct regulators in cycling progenitors or deuterosomal cells. We found that in addition to *Cdk1*, *Ccnb1*, APC/C subunits, and *Cdc20*, nearly all mitotic oscillator components are re-expressed in deuterosomal cells to levels significantly comparable to those in cycling progenitors (Figures 2C and 2D), showing that the whole machinery is co-opted and refuting the hypothesis that mitotic clock attenuation in MCCs is driven by a global decreased expression of the mitotic oscillator components. However, several APC/C inhibitors are re-expressed in differentiating MCCs at lower levels than in cycling progenitors. Notably, the APC/C inhibitor *Emi1/Fbxo5* is totally silenced (see Figures 2C, 2D, and S4B). It is replaced by its homolog *Emi2/Fbxo43*, albeit expressed at very low levels (Figure S4C), consistent with a role of *Emi2* in MCC differentiation previously documented in *Xenopus*.⁵ This indicates that an overactive APC/C, rather than decreased expression of the mitotic oscillator main components, might attenuate the mitotic clock in MCC.

Altogether, these results show that a large proportion of genes from all the cell division processes are re-expressed in differentiating mouse MCCs and, therefore, suggest that in addition to centriole biogenesis, cell-cycle-like reorganization of the cytoplasm, the nuclear membrane, and even the chromatin occurs during MCC differentiation. Further studies are needed to highlight the other aspects of the cell cycle that are co-opted to control MCC differentiation.

Deuterosomal cells progress through differentiation by following a transcriptional circular trajectory similar to the cell cycle

The expression of the cell cycle regulatory circuitry in deuterosomal cells suggests that they can progress through the different intermediate stages of differentiation by using regulatory mechanisms thought to be restricted to cycling cells progressing through different cell cycle phases. Supporting this, when processed together, deuterosomal cells cluster with cycling

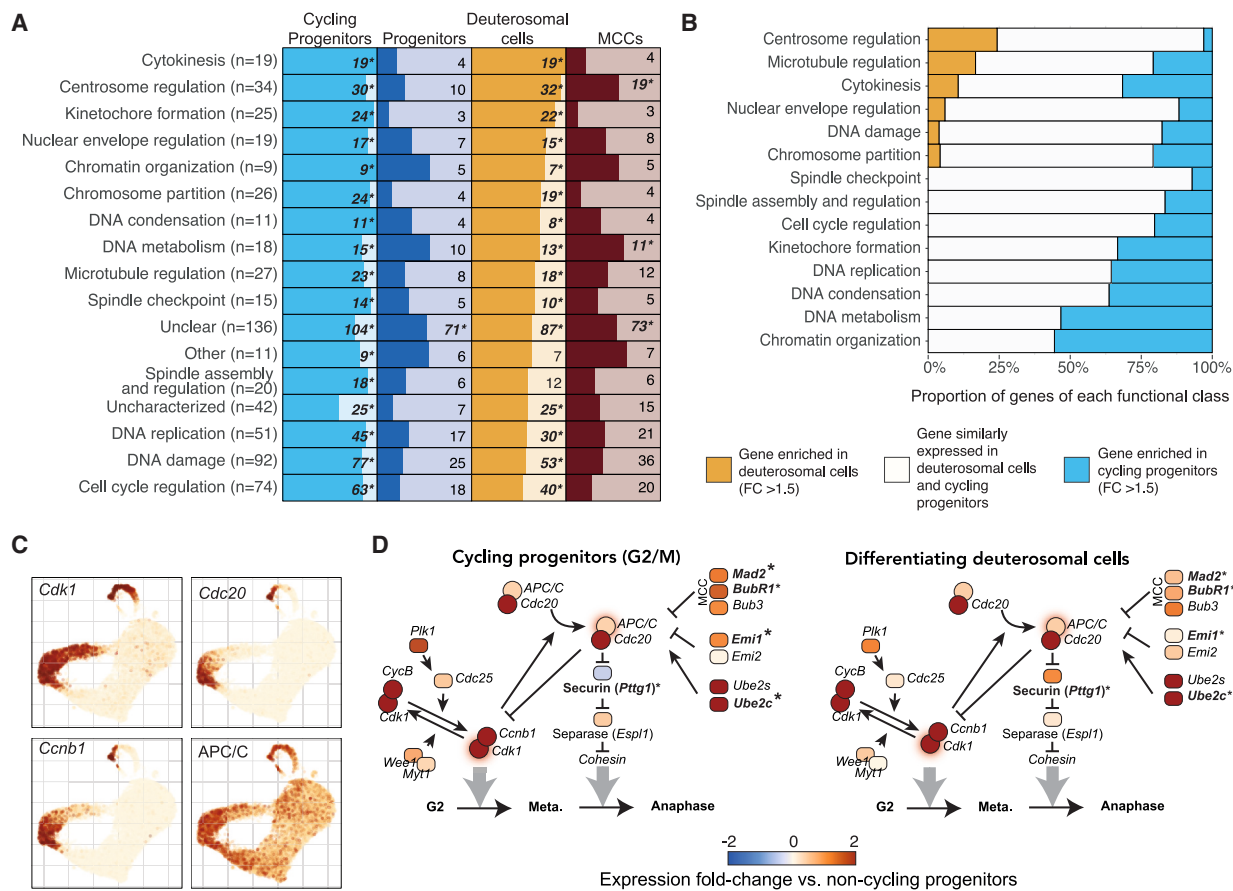


Figure 2. Factors from all cell cycle subprocesses are re-expressed in deuterosomal cells

(A) Table of cell cycle factors expressed in each cell population. Cell cycle factors were manually classified by their main function in the cell cycle.¹⁴ Stars denote cell cycle functions statistically enriched (>4-fold, $p < 0.01$) for genes expressed in cycling progenitors, post-mitotic progenitors, deuterosomal cells, or MCCs. The total number of factors in each functional class is indicated in parentheses.

(B) Proportion of cell cycle factors preferentially enriched in deuterosomal cells versus cycling progenitors (orange) or cycling progenitors versus deuterosomal cells (in blue) or not differentially expressed (in white). Genes that are not detected in any of the two cell populations are not included.

(C) UMAP of the scRNA-seq dataset, each cell colored by the level of expression of *Cdk1*, cyclin B (*Ccnb1*), *Cdc20*, or the average expression of all APC/C subunits.

(D) Schematic of the main components of the mitotic oscillator in G2/M cycling progenitor cells (left) or deuterosomal cells (right). The colormap indicates gene expression fold change versus non-cycling progenitor cells. Labels in bold indicate factors differentially expressed between deuterosomal cells and G2/M cycling progenitors (abs. fold change > 1.5, $p < 0.01$).

See also Figure S4.

progenitors according to their putative cell cycle phase (Figures S5A–S5D).

Several reports recently showed that a stereotypical clocklike progression of cells through the cell cycle can be identified from scRNA-seq data.^{15–17} Schwabe et al. and Zinov'yev et al. both revealed that immortalized cycling cells embedded in a linear principal-component analysis (PCA) space form a circular path along which they advance as a cycle.^{16,17} PCA integration of our primary cycling progenitors ($n = 759$ cells) highlighted that these cycling primary cells also form a planar circular path in linear two-dimensional (2D) space (Figure 3A). We computed a radial progression for each cell, which we used to reveal that cell cycle phases are sequentially distributed along this circular path (Figure 3B), confirming previously published results in immortalized

cycling cells. We then performed the same analysis on deuterosomal cells and observed that they recapitulate a similar circular path, successively traversing early, mid, and late deuterosomal transcriptional stages (Figures 3C and S5E). Importantly, we found that putative cell-cycle-like phase annotations for deuterosomal cells are also sequentially distributed along the circular trajectory (Figure 3D), as shown for cycling progenitor cells. Deuterosomal cells radially progress through G0/G1-, S-, G2-, and M-like phases, albeit with a relative enrichment of S/G2- and G2/M-like cells over pure S-like cells when compared to the cycling progenitors. This lower representation of S-like cells is consistent with the lower number of DNA replication factors being re-expressed in deuterosomal cells (Figures 2A, 2B, and S4A).

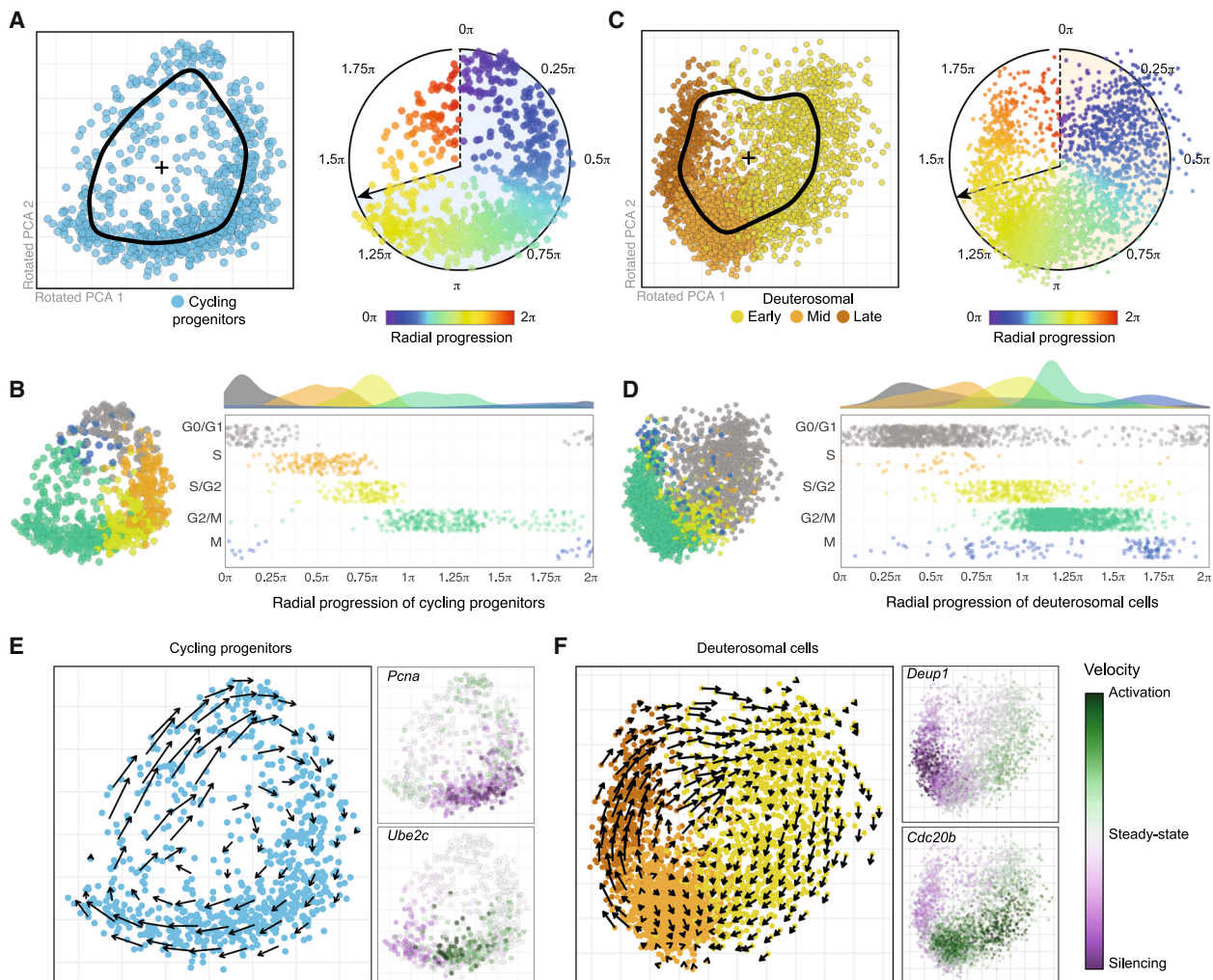


Figure 3. Deuterosomal cells progress through differentiation following a cell-cycle-like circular trajectory

(A) PCA embedding (PC1 and PC2) of cycling progenitor cells. The black curve denotes the average position of cells around the center point of the PCA space. Right: representation of the cycling progenitors with a color range indicating the radial progression of each cell.

(B) Radial distribution of cycling progenitors with a color scale indicating the putative cell cycle phase annotated using SingleR and a neural stem cell reference.¹¹

(C) PCA embedding (PC1 and PC2) of deuterosomal cells. The black curve denotes the average position of cells around the center point of the PCA space. Right: representation of the deuterosomal cells with a color range indicating the radial progression of each cell.

(D) Radial distribution of deuterosomal cells with a color scale indicating the putative cell cycle phase annotated using SingleR and a neural stem cell reference.¹¹

(E) RNA velocity analysis of cycling progenitors and deuterosomal cells. RNA velocity relies on nascent transcript abundance to predict where each cell would be positioned in the future. Left: RNA velocity vector field of cycling progenitor cells. Right: RNA velocity score for *Pcna* and *Ube2c*, two cell-cycle-related genes.

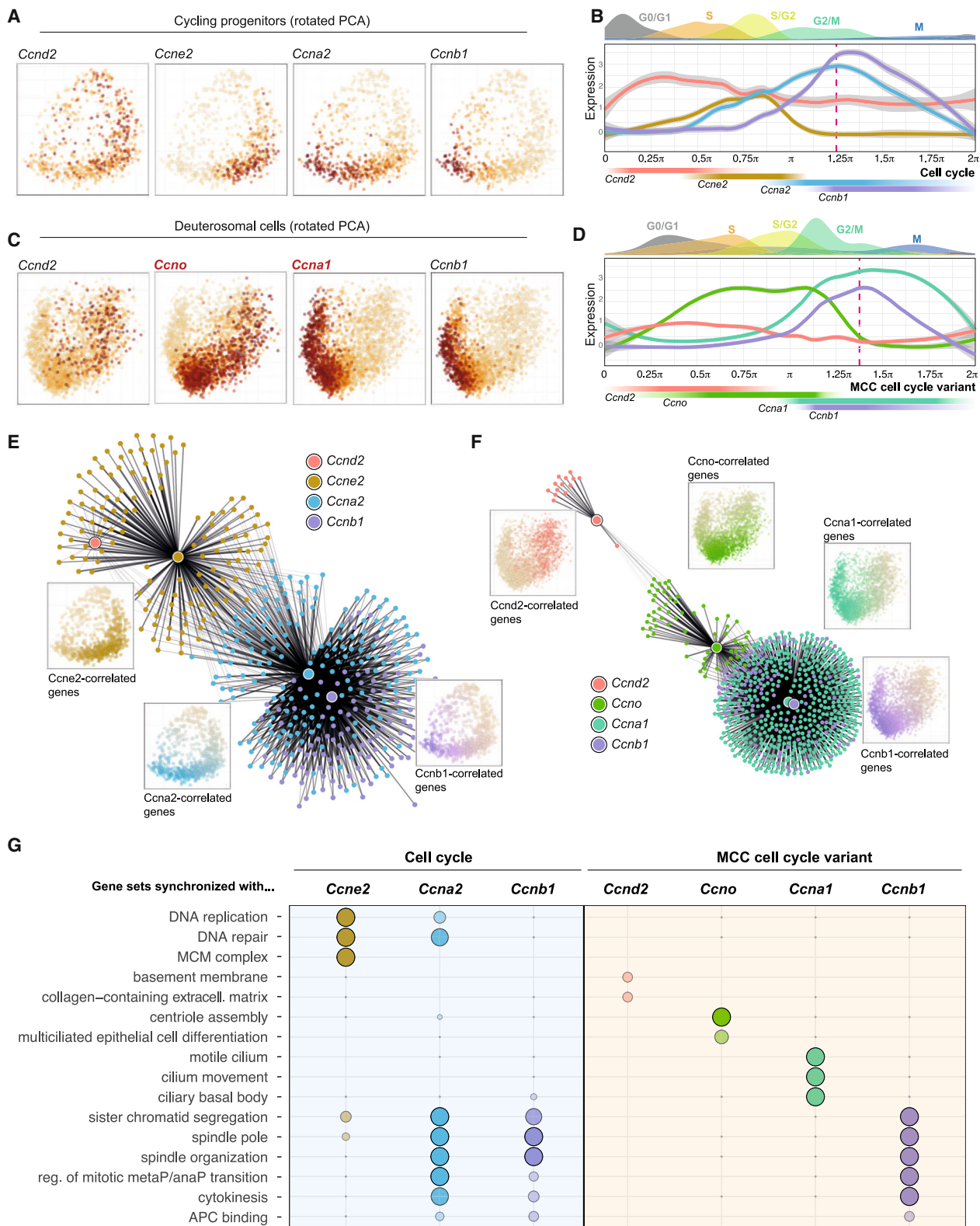
Green (purple) indicates an increasing (decreasing) production of nascent RNA, while white indicates a steady-state production of nascent RNA.

(F) Left: RNA velocity vector field of deuterosomal cells. Right: RNA velocity score for *Deup1* and *Cdc20b*, two genes involved in the regulation of MCC differentiation.

See also Figure S5.

We then computed RNA velocity in each subset of cells.¹⁸ In both cycling progenitors and deuterosomal cells, the RNA velocity vector field reveals that cells move forward (i.e., clockwise) along their circular path (Figures 3E and 3F). RNA velocity scores of genes transiently transcribed during the cell cycle (e.g., *Pcna* or *Ube2c*) or MCC differentiation (*Deup1* and *Cdc20b*) confirmed that transcription of these genes sequentially occurs along the respective cycling and deuterosomal circular paths.

In agreement with what has been previously described in immortalized cell lines¹⁶ and with our own measurements in cycling progenitors, we also observed a gradual increase in (1) the number of expressed genes and (2) the total transcript content in deuterosomal cells during the S- and G2-like phases up to a tipping point, after which transcription is reduced, as seen in cycling cells after mitosis entry (Figure S5F). Also, similar to what has been previously described in immortalized cycling cell lines¹⁶ and what we observe in primary cycling progenitors,



(legend on next page)

we found two regimes of gene transcription onsets in deuterosomal cells: first a relatively fast rate for 96% of the genes variably expressed in deuterosomal cells (2,106/2,183), followed by a stark decrease (~4.5-fold decrease) shortly before the cells reach their maximum transcriptional output ([Figure S5G](#)).

Altogether, these results show that brain differentiating MCCs share all the features of transcriptional regulation previously characterized in cycling cells. They follow a multiciliation trajectory characterized by successive cell-cycle-like phases and reuse the optimized principles of cell cycle gene regulation. We observed a similar distribution of cell-cycle-like transcriptional signatures along a circular trajectory of deuterosomal cells during *in vivo* mouse embryonic brain development¹² ([Figures S5H–S5J](#)). We conclude that the differentiation lineage of MCCs consists of a single iteration of a cell cycle variation.

A cascade expression of cyclins characterizes the MCC cell cycle variant

Cyclins are the key factors controlling the progression of cycling cells through the cell cycle. When a cyclin accumulates to a sufficient threshold, it acts as a molecular switch that triggers the enzymatic activity of specific cyclin-dependent kinases. It has been established that (1) D-type cyclins are involved in progression through the G1 phase, (2) E-type cyclins contribute to the transition from the G1 to the S phase, (3) cyclin A2 orchestrates interphase progression as well as the G2/M transition, and (4) cyclin B1 controls progression from entry to exit of mitosis.¹⁹ Successive waves of cyclin expression provide a tentative model to organize the MCC cell cycle variant.

Leveraging the cyclic progression of proliferating progenitor cells, we modeled the temporal activation of canonical cyclins in cycling cells, which recapitulated the well-known expected pattern of successive waves of cyclin transcription, with D2, E2, A2, and B1 cyclins broadly delineating the different putative cell cycle phases ([Figures 4A and 4B](#)). This result confirms that the radial distribution of dividing cells along a scRNA-seq circular trajectory can be used to estimate cell cycle progression in proliferating progenitors ([Figure 4B](#)). Then, using the same approach in deuterosomal cells, we found that cyclins D2 (*Ccnd2*) and B1 (*Ccnb1*) were transiently expressed in the MCC cell cycle variant ([Figures 4C and 4D](#)). The temporal expression profiles of these two cyclins were highly correlated with those from cycling pro-

genitors ($r = 0.98$ for *Ccnd2* and $r = 0.97$ for *Ccnb1*), albeit with an expression generally lower for *Ccnd2* ([Figure 4D](#)). In contrast, the other canonical cyclins (i.e., A2 and E-type cyclins) remained mostly untranscribed throughout this cell cycle variant. Instead, cyclins O (*Ccno*) and A1 (*Ccna1*), previously shown to be involved in MCC differentiation,^{4,20,21} are as highly expressed as *Ccnd2* and *Ccnb1* in the MCC cell cycle variant ([Figures 4C, 4D, and S6A](#)).

Importantly, we uncovered that their expression patterns were temporally delimited, defining two different periods for which each cyclin is predominantly expressed. *Ccno* is prominently expressed from the S- and up to the G2/M-like phase of the MCC cell cycle variant, while *Ccna1* is mostly expressed during the G2/M- and M-like phases ([Figure 4D](#)). In addition, the temporal expression patterns of *Ccno* and *Ccna1* in deuterosomal cells are correlated with those of *Ccne2* and *Ccna2* in cycling progenitors, respectively ($r = 0.83$ and 0.62). Importantly, we observed a similar temporality of successive cyclin expression along MCC differentiation, both during *in vivo* mouse embryonic brain development ([Figure S6B](#))¹² and in the human epithelial airway ([Figure S6C](#)).²² Altogether, these results show that MCC differentiation is marked by successive, partially overlapping, waves of cyclin transcription, analogous to those described in the cell cycle, with sequential D2, O, A1, and B1 cyclin phases, further supporting the existence of a genuine cell cycle variant during MCC differentiation.

Waves of cyclin expression segment the cell cycle into successive phases. In each phase, functional sets of genes are predominantly expressed to carry out specific biological functions in each cell cycle phase.^{23,24} Indeed, we found hundreds of genes whose temporal expression was positively correlated with that of canonical cyclins within the cell cycle ($n = 130$ genes with highest correlation for cyclin E2, $n = 187$ for cyclin A2, $n = 110$ for cyclin B1) ([Figure 4E](#)). The functions of these gene sets are respectively enriched for replication processes (minichromosome maintenance (MCM) complex, nuclear DNA replication), mitosis regulation (e.g., centrosome regulation, spindle checkpoint), and late-mitosis events (e.g., APC/C activity), confirming that cyclin-correlated patterns of temporal expression allow defining groups of genes that are functionally related to the cyclin ([Figure 4G](#)). The same analysis performed on deuterosomal cells pointed at hundreds of genes with expression positively

Figure 4. Deuterosomal cells activate cascades of canonical and non-canonical cyclins with coordinated gene expression

- (A) Expression of cyclin D2 (*Ccnd2*), cyclin E2 (*Ccne2*), cyclin A2 (*Ccna2*), and cyclin B1 (*Ccnb1*) canonical cyclins in cycling progenitor cells in PCA embedding.
 - (B) Expression of these cyclins in cycling progenitors distributed according to their radial progression. This recapitulates the well-known pattern of successive waves of cyclin expression during the cell cycle.
 - (C) Expression of cyclin D2 (*Ccnd2*), cyclin O (*Ccno*), cyclin A1 (*Ccna1*), and cyclin B1 (*Ccnb1*) cyclins in deuterosomal cells in PCA embedding.
 - (D) Expression of these cyclins in deuterosomal cells distributed according to their radial progression. Note the successive waves of *Ccnd2*, *Ccno*, *Ccna1*, and *Ccnb1* expression, resembling the waves of canonical cyclin expression in cycling progenitors.
 - (E) Network of genes (small nodes) whose temporal expression correlates with that of canonical cyclins (larger nodes) in cycling progenitor cells. The colors indicate with which cyclin each gene is mostly correlated. Edge thickness is proportional to the correlation score between gene expression and cyclin expression. Only correlations greater than 0.3 (Pearson p score) are shown. Insets show the average expression of all the genes correlated with each cyclin during the canonical cell cycle.
 - (F) Same as in (E) but for cyclins expressed with deuterosomal genes. Insets show the average expression of all the genes correlated with each cyclin during the MCC cell cycle variant.
 - (G) Biological functions associated with sets of genes temporally correlated with each cyclin in cycling progenitors (left) or deuterosomal cells (right). Genes with a p correlation score greater than 0.3 for several cyclins were associated with the cyclin with which they had the greatest correlation.
- See also [Figure S6](#).

correlated with that of cyclin O ($n = 60$), cyclin A1 ($n = 499$), or cyclin B1 ($n = 115$) (Figure 4F). Genes mostly correlated with cyclin B1 were involved in mitosis events, and some components have been involved in centriole number, growth, and disengagement³ (Figure 4G). Genes mostly correlated with cyclin O appear enriched for key MCC differentiation and centriole biogenesis regulators, while those mostly correlated with cyclin A1 are enriched for cilium biogenesis and motility, which contradicts recent data suggesting an early involvement of this CCNA1 in centriole amplification.⁴ Interestingly, we found the same consecutive expression of *Ccno* and *Ccna1* and the same switch between *Emi1* and *Emi2* expression during male meiosis²⁵ (Figures S6D and S6E), another important cell cycle variant during which centriole biogenesis occurs—in the absence of DNA replication—and is followed by motile flagella growth.

Altogether, these results support the existence of an MCC-specific cell cycle variant, supported by successive waves of cyclin expression, in which the cell cycle deviates from its expected trajectory by replacing some canonical cyclins with non-canonical ones. In this variant conserved across tissues and mammals, the onset is marked by the expression of *Ccno* instead of *Ccne2*, consistent with an increase in cytoplasmic centriole content instead of nuclear ploidy. Later, and with the same temporality as in the cell cycle, *Ccnb1* is expressed, consistent with the role of the mitotic oscillator in centriole growth and disengagement.³ During a comparable period, *Ccna1* is expressed instead of the second mitotic cyclin, *Ccna2*, and its expression is correlated with genes involved in cilia motility.

Expression of canonical cyclins E2 or A2 and/or APC/C inhibitor Emi1 can trigger cell cycle nuclear events

We next hypothesized that if MCC differentiation is a valid cell cycle variant, then re-expression of the missing canonical elements would restore the nuclear events skipped during differentiation. In particular, *Emi1*—an APC/C inhibitor that regulates the progression of the canonical cell cycle by regulating DNA replication and its coupling to mitosis^{26–28}—is drastically silenced during MCC differentiation and partially replaced by its homolog *Emi2*, lowly expressed in deuterosomal cells (Figures S4C and S6A). We should be able to restore DNA replication and/or mitotic events specifically in differentiating cells by re-expressing missing EMI1. Supporting this hypothesis, a recent study in *Xenopus* reported EdU incorporation and mitosis figures in differentiated skin MCCs upon APC/C inhibition by the overexpression of *Emi2*.⁵ We infected differentiating cells to express the missing *Emi1* and monitored DNA replication by EdU incorporation and mitosis entry by immunostaining phosphorylation of histone 3 serine 10 (H3S10p) (see STAR Methods). We observed a partial replication in a subset of differentiating progenitors at 96 h post-infection (hpi) (Figures 5A and 5C), which we failed to detect upon infection with GFP or with *Emi1* at 24 hpi (Figures 5C and S7A). We also detected a significant proportion of differentiating MCCs with mitotic figures—marked by chromosome condensation, nuclear envelope breakdown, and actin network remodeling—upon *Emi1* infection, both at 24 and 96 hpi (Figures 5B, 5C, S7B, and S8). This suggests that the silencing of EMI1, and more generally, the decreased expression of APC/C inhibitors (Figures 2B and S4B), is a phys-

iological explanation for the dampening of CDK1 activity, which was previously shown by pharmacological treatments to be responsible for the decoupling between cytoplasmic and nuclear processes preventing mitotic events in differentiating MCCs.³ This dampening seems to also be involved in preventing DNA replication.

Cyclins E2 and A2 are two other cell cycle core regulators not reactivated during MCC differentiation. Cyclin E2 is required for the transition between G1 and S and the initiation of replication, whereas cyclin A2 is crucial for the correct progression through S and G2 phases up to mitosis entry.^{29,30} We infected cells with cyclin E2 and cyclin A2 and monitored DNA replication and mitosis entry events. We observed that cyclin E2 infection was sufficient to induce partial DNA replication in some differentiating cells, marked by foci of incorporated EdU 96 hpi (Figures 5A, 5D, and S7C). The co-infection of cyclin E2 with *Emi1* doubled the proportion of EdU-positive deuterosomal cells, suggesting an additive effect of each factor. On the other hand, we observed that cyclin A2 infection was sufficient to induce mitotic events in some differentiating cells 24 hpi (Figures 5A, 5D, and S7C), and the co-infection of cyclin A2 with *Emi1* dramatically increased the number of differentiating MCCs entering mitosis. This synergistic effect is likely due to EMI1-dependent inhibition of APC/C, which is normally involved in cyclin A degradation, leading to the indirect stabilization of ectopic cyclin A2, as shown by the increase in cyclin A2-positive differentiating cells upon co-infection (Figure S7D).

Interestingly, although critical elements of the cytokinesis control machinery are re-expressed in deuterosomal cells (Figure S4), cytoplasmic division was never observed, perhaps because a combination of biochemical and mechanical signals drives it. Also, full DNA replication was not observed, suggesting that some factors are missing for complete DNA synthesis, as suggested by our previous observations (Figure S4) and a parallel study.¹⁰ Strengthening this hypothesis, the partial replication we observe is systematically located at the periphery of chromocenters (Figure S9A), and elements of the replisome recently involved in centromere replication (e.g., TOP2A topoisomerase, the SMC5/6 structural maintenance complex, or polymerase subunits, e.g., polymerase ζ subunit Rev3l or polymerase α subunits $\alpha 1$ and $\alpha 2$)³¹ are re-expressed or remain expressed during differentiation (Figure S9B).

Overall, these results confirm that MCC differentiation is a genuine cell cycle variant. They also show that it is tailored by variation in cyclin and APC/C inhibitor expression to allow centriole biogenesis without associated nuclear replication and mitosis. In a follow-up study, we investigate the role of cyclin O, the first non-canonical cyclin expressed during the MCC cell cycle variant.⁹

DISCUSSION

A cell cycle variant orchestrates MCC differentiation

Cell cycle variants can diverge from the G1-S-G2-M phases of the canonical cell cycle. Some cells can skip DNA replication to make haploid gametes in meiosis or accelerate cell division during asynthetic fission,³² while others can skip mitotic cell division to increase the genomic content of differentiating cells

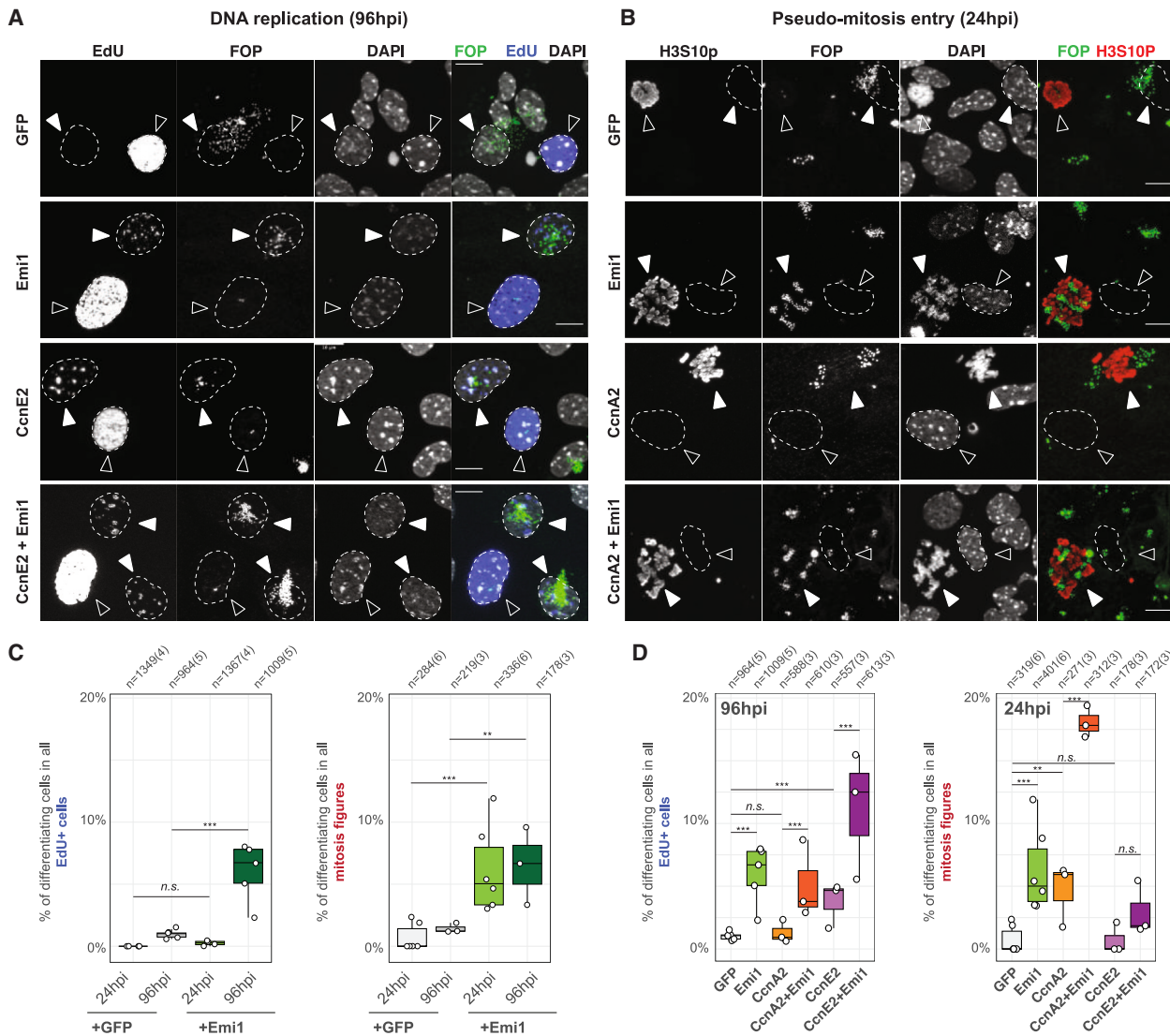


Figure 5. Reactivating APC/C inhibitor Emi1 or the canonical cyclins E2 or A2 can rescue cell cycle nuclear events

(A) Representative images of cells infected to express different combinations of cell cycle factors, stained for EdU incorporation (96 hpi). Centriole staining by FOP is used to identify progenitors (black arrows) and differentiating deuterosomal cells (white arrows). Scale bar: 10 μ m.

(B) Representative images of cells infected to express different combinations of cell cycle factors, immunoassayed for mitosis figures (with H3S10p) (24 hpi). Centriole staining by FOP (FGFR1 oncogene partner) is used to identify progenitors (black arrows) and differentiating deuterosomal cells (white arrows). Scale bar: 10 μ m.

(C) Proportion of differentiating deuterosomal cells among all the cells marked by EdU (left) or mitosis figures (right), after GFP or Emi1 overexpression, 24 and 96 hpi. Differentiating deuterosomal cells are identified according to FOP staining. The total number of cells counted for each experiment is indicated on top of each boxplot, with the number of replicates indicated in parentheses. Full counts are provided in Table S2. Cultures for each replicate were performed by pooling cells from 1–6 newborn mice. Counts were performed by scanning over a coverslip and visually enumerating relevant cells. p values are calculated using a Fisher's exact test and summarized as follows: * p < 0.05, ** p < 0.01, and *** p < 0.001. Boxplots show the median (horizontal line), the interquartile range (IQR; represented by the height of the box, spanning from the 25th to the 75th percentile), and the whiskers extend from the box to the smallest and largest values within 1.5 times the IQR from the lower and upper quartiles, respectively.

(D) Same as (C) but with additional infections by Ccne2, Ccne2+Emi1, Ccna2, or Ccna2+Emi1. Counts for EdU incorporation were performed 96 hpi. Counts for mitosis figures were performed 24 hpi. Counts for GFP and Emi1 infections are the same as those shown in (C) for easier comparison with the other conditions. Boxplots representations are the same as in (C).

See also Figures S7–S9.

(endoreplication³³). Here, we show that MCC differentiation is a final and customized iteration of the cell cycle skipping both DNA replication and mitotic division to drive the amplification of cytoplasmic organelles, the centrioles (Figure 6). We propose this

process to be a genuine variation of the cell cycle since we show that cells differentiating into MCCs (1) organize their transcriptome in a circular trajectory, (2) progress through S-, G2-, and M-like phases along this circular trajectory, (3) progressively

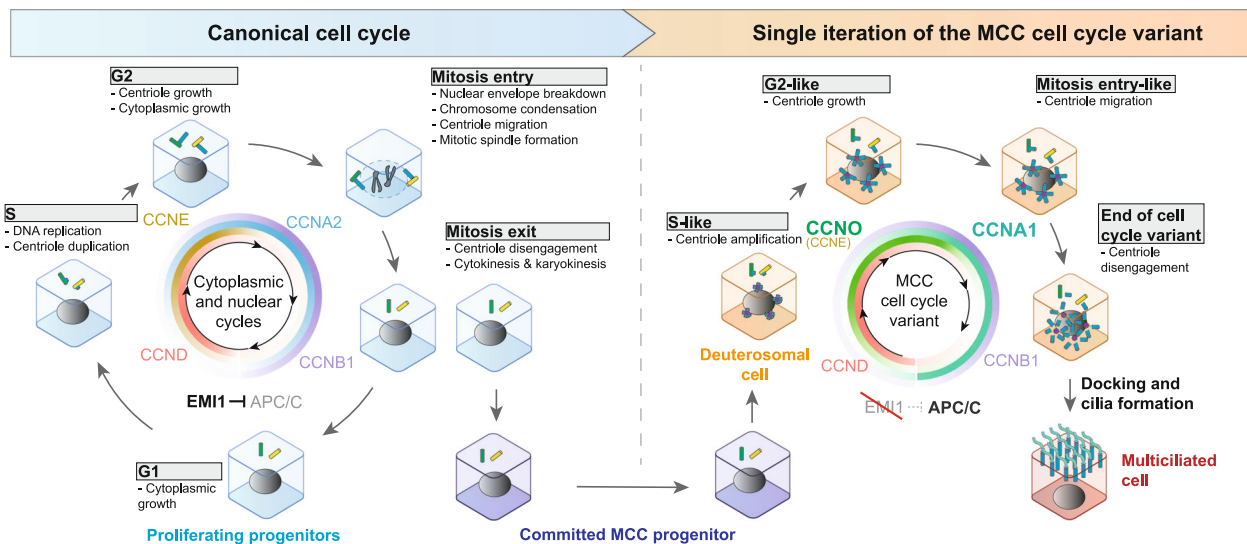


Figure 6. MCC differentiation is a final iteration of a genuine cell cycle variant

In both the canonical cell cycle (left) and the MCC cell cycle variant (right), cells organize their transcriptome in a circular trajectory, progress through S-, G2-, and M-like phases along this circular trajectory, progressively increase their transcriptional output, followed by a sharp decline when they enter G2/M-like phase, and are marked by waves of cyclins that demarcate consecutive functional phases along this circular trajectory. However, in the MCC cell cycle variant, the expression of cyclins E2 and A2, correlated, respectively, with the expression of DNA replication and mitosis regulators in the canonical cycle, is replaced by the expression of non-canonical cyclins O and A1, correlated, respectively, with the expression of centriole and motile cilia genes. Also, the primary APC/C inhibitor *Emi1* is silenced. Re-expressing these missing elements can rescue cell cycle nuclear events. We propose that such adaptation of the cell cycle genetic program diverts CDK activity toward the cytoplasmic rearrangement required for multiciliation (see Figure S10). Note tissue specificity for (1) D-type cyclins, with cyclin D1 predominantly expressed in respiratory cells, while cyclin D2 is predominantly expressed in brain cells,¹⁰ and (2) E-type cyclins, which are silenced in the brain MCC cell cycle variant, while they remain expressed in the respiratory MCC cell cycle variant.¹⁰

See also Figure S10.

increase their transcriptional output, followed by a sharp decline when they enter the G2/M-like phase, and (4) are marked by waves of cyclins that demarcate consecutive functional phases along this circular trajectory. This variant is marked by the replacement of some core cyclins with atypical ones and by the silencing of *Emi1*, the primary APC/C inhibitor. Re-expression of these missing canonical elements can restore partial DNA replication, full DNA condensation, and nuclear envelope breakdown. A parallel study in respiratory MCCs shows that an additional non-canonical player, the transcription factor E2F7, is also expressed, which downregulates some DNA duplication players, and participates in DNA replication block.¹⁰

The MCC cell cycle variant is quantitatively regulated

The canonical cell cycle is regulated by two complementary principles: a quantitative increase in CDK activity driving progression through cell cycle phases, as well as a qualitative specificity of substrates of CDK activity influenced by cyclins.³⁴ In particular, different thresholds of CDK activity are proposed to exist: a lower CDK activity threshold required for DNA replication during the S phase, and a higher CDK activity threshold required for entry into mitosis.³⁵ This allows a decoupling between different cell cycle events. For example, cells undergoing endoreplication differ from dividing cells by their inability to segregate chromosomes or divide, and this would be partly driven by a tuning of CDK activity allowing the cell to progress through the S but not the M phase.³³ In addition, experimental dampening of CDK activity

in cycling cells can block nuclear events while staying permissive from cytoplasmic ones,^{36,37} such as centriole biogenesis.³⁸ In a previous report, we have already shown that pharmacologically blocking CDK1 inhibitory phosphorylation by Wee1/Myt1 in differentiating MCCs resulted in nuclear mitotic events, highlighting that CDK activity is normally dampened in differentiating MCCs to avoid mitosis.

Here, we further show that the core repressor of APC/C, *EMI1*, is missing in the MCC cell cycle variant and that its re-expression can trigger partial DNA replication and mitotic-like events. A previous study focusing on differentiating skin MCCs in *Xenopus* also showed that the overexpression of *Emi2*, an *Emi1* homolog, also leads to DNA replication and mitotic events.⁵ Our results, together with previous reports, suggest that MCC differentiation relies on the existence of another CDK activity threshold, even lower than the DNA replication threshold and maintained by the controlled expression of cyclins and APC/C inhibitors *Emi1/2*, that is permissive for centriole amplification but not DNA replication nor mitosis entry (Figure S10). This attractive hypothesis remains to be tested, for example by performing inducible degradation of cyclins or CDKs specifically in the cytoplasmic or nuclear compartment. Other mechanisms could also contribute to the decoupling between the nuclear and cytoplasmic compartments; for example, controlled cyclin translocation into the nuclear compartment³⁹ or a greater affinity of cyclin-CDKs to cytoplasmic cell cycle factors (e.g., centrioles) than to nuclear targets.

The MCC cell cycle variant is qualitatively regulated

In this study, we also highlight that while the core cell cycle machinery is present, the E2 and A2 cyclins are, respectively, replaced by the non-canonical O and A1 cyclins. The two non-canonical cyclins are expressed in different differentiation time frames, and their temporal expression is correlated with that of gene sets with different functions related to MCC differentiation. In addition, rescuing the activity of the canonical cyclins E2 and A2 can be sufficient to reroute differentiating cells toward cell-cycle-like events. Interestingly, *Ccne1* is more expressed than *Ccne2* in tracheal cells and remains expressed in tracheal deuterosomal cells,¹⁰ suggesting differences between mouse tissues as also reported in our companion report.⁹ More importantly, we have further characterized the role of the non-canonical cyclin O in this MCC cell cycle variant in a follow-up study.⁹ We reveal that CCNO is required to progress through the G1-to-S transition of the MCC cell cycle variant. This shows that a qualitative control, in addition to the APC/C-mediated quantitative regulation of CDK activity, orchestrates centriole amplification rather than DNA replication and mitosis in MCC (Figure S10). Of note, the expression of these cyclins in two distinct waves, with cyclin O ahead of cyclin A1, contrasts with what has been suggested during MCC differentiation in respiratory cells.⁴ This could be explained by the great increase in the resolution of the progression of differentiation achieved by scRNA-seq in our study. In conclusion, a nearly identical cell cycle machinery with identical transcriptional oscillations but different sets of cyclins orchestrates the MCC cell cycle variant, whose cellular outcome is entirely different from cell division.

Interestingly, we also identified successive expression of the non-canonical cyclins O and A1 as well as the tuned expression of *Emi2*, replacing *Emi1*, in male meiosis, an essential variant of the canonical cell cycle where centrioles are produced uncoupled from DNA replication.^{40–42} The wave-like expression of *Ccno* is also associated with the transcriptional silencing of *Ccne2* during male meiosis, further reinforcing the relevance of the MCC differentiation program as a genuine cell cycle variant regulated both qualitatively and quantitatively.

Relevance of the MCC cell cycle variant in pathologies

While such proximity between cell division and centriole amplification may appear risky,¹ this cell cycle variant—marked by the association of centriole amplification with low CDK activity—could be an efficient barrier to avoid DNA replication and cell division in cells with amplified centrioles. Supporting this “failsafe” hypothesis, several medical reports reveal the existence of MCCs in cysts that have been found in a wide variety of normally non-multiciliated organs (2,202 occurrences of the term “ciliated cyst” in the PubMed database, e.g., in Fernández Figueiras et al.,⁴³ Rubio et al.,⁴⁴ and Hughes et al.⁴⁵). Such potential for multiciliation in a progenitor cell could also underpin the observed formation of MCCs along the lumen of non-MCC fluid-producing tissues (kidney, urethra) in pathological situations, where they could contribute to restore fluid flow.^{46–48} On the other hand, such proximity between canonical and MCC cell cycle variants may lead to altered MCC epithelia integrity in respiratory and/or reproductive organs in patients treated with chemotherapies. In addition to providing a detailed prism

for the study of multiciliation mechanisms, the close similarity of multiciliated differentiation mechanisms to those of the cell cycle revealed in this study expands the putative functions of MCCs, sheds new light on the link between centriole number and cell division, and shows that cell cycle variants can also control cytoplasmic and not only nuclear processes during cell differentiation.

Limitations of the study

In this study, we focus on the transcriptional regulation of cell cycle factors during the MCC cell cycle variant. We have already shown that upon pharmacological induction, differentiating cells could enter pseudo-mitosis in 30 min, including full chromosome condensation, nuclear envelope breakdown, and microtubule reorganization.³ This suggests that transcripts encoding mitosis factors are indeed translated into protein. However, the post-translational regulation of cell cycle factors by phosphorylation or proteolysis is fundamental for progression through the canonical cell cycle phases and could also contribute to the regulation of cell cycle processes during MCC differentiation, which could contribute to the partial rescue when re-expressing *Ccne2* or *Emi1*. Since MCC differentiation initiates asynchronously within a population of cycling progenitors and could not be synchronized, investigating the mechanisms of post-translational regulation would need the application of emerging single-cell proteomics and phosphoproteomics approaches. This next step would greatly help to untangle the regulatory mechanisms controlling this cell cycle variant.

RESOURCE AVAILABILITY**Lead contact**

Requests for further information and resources should be directed to and will be fulfilled by the lead contact, Alice Meunier (alice.meunier@bio.ens.psl.eu).

Materials availability

This study did not generate new unique reagents.

Data and code availability

- Raw and processed sequencing data have been deposited at the NCBI Gene Expression Omnibus under the accession ID GEO: GSE201773 (GEO; <https://www.ncbi.nlm.nih.gov/geo/>) and are publicly available as of the date of publication. Accession numbers are listed in the [key resources table](#). Processed scRNA-seq data are also available for interactive investigation using the CELLxGENE platform (collection # 33f48a52-31d8-4cc8-bd00-1e89c659a87f) at <https://cellxgene.cziscience.com/collections/33f48a52-31d8-4cc8-bd00-1e89c659a87f> as of the date of publication.
- All original code has been deposited at Zenodo (record #14105247) and is publicly available at <https://doi.org/10.5281/zenodo.14105247> as of the date of publication. The Zenodo accession numbers are also listed in the [key resources table](#).
- Any additional information required to reanalyze the data reported in this paper is available from the [lead contact](#) upon request.

ACKNOWLEDGMENTS

We thank all members of the Spassky and Koszul labs for fruitful discussions and comments on the manuscript and Andrew Holland and Damien Coudreuse for reading and discussing the manuscript. We are grateful to Kévin Lebrigand and Virginie Magnone for constructive discussions on single-cell RNA sequencing, the IBENS administrative staff, and the animal facility for animal

care. This work is supported by funding to A.M. and R.K. from Agence Nationale pour la Recherche (Q-Life program and ANR-19-CE13-0027 grant). R.K. is also supported by the Institut Pasteur, CNRS, and the European Research Council (ERC) under the European Union's Horizon 2020 (ERC grant agreement 771813). The Spassky laboratory is also funded by INSERM, the CNRS, the Ecole Normale Supérieure (ENS), the ANR (ANR-20-CE45-0019, ANR-21-CE16-0016, and ANR-22-CE16-0011) the ERC (ERC consolidator grant 647466, N.S.) and Fondation pour la Recherche Médicale (FRM EQU202103012767). J.S. is funded by Association pour la Recherche sur le Cancer; M.K.D. is funded by Fondation pour la Recherche Médicale; A.-R.B. is funded by La Ligue Contre Le Cancer; and R.B. is funded by Q-Life. This work was performed with support from the National Infrastructure France Génomique (Commissariat aux Grands Investissements, ANR-10-INBS-09-03 and ANR-10-INBS-09-02), the 3IA Côte d'Azur (ANR-19-P3IA-0002), European Union's Horizon 2020 Research and Innovation Programme under grant agreement no. 874656 (discovAIR), Fondation pour la Recherche Médicale (DEQ20180339158), and Conseil départemental 06 (2016-294DGADSH-CV). We thank Camille Noûs, a collective of researchers, who encouraged us to maintain open, honest and slow science.

AUTHOR CONTRIBUTIONS

Conceptualization, J.S., R.K., and A.M.; methodology, J.S., A.-R.B., M.F., and N.D.; software, J.S.; formal analysis, J.S.; investigation, J.S., A.-R.B., M.K.D., R.B., L.-E.Z., N.S., and A.M.; resources, A.-R.B., M.K.D., M.F., N.D., N.S., and A.M.; visualization, J.S.; funding acquisition, P.B., N.S., R.K., and A.M.; project administration, R.K. and A.M.; supervision, R.K. and A.M.; writing – original draft, J.S., R.K., and A.M.; writing – revised draft, J.S. and A.M.

DECLARATION OF INTERESTS

The authors declare that they have no competing interests.

STAR METHODS

Detailed methods are provided in the online version of this paper and include the following:

- KEY RESOURCES TABLE
- EXPERIMENTAL MODEL AND STUDY PARTICIPANT DETAILS
 - Animals
- METHOD DETAILS
 - Single-cell RNA-seq of *in vitro* differentiating multiciliated cells
 - Adenovirus infections
 - Immunostainings and EdU incorporation stainings
 - Computational analyses
- QUANTIFICATION AND STATISTICAL ANALYSIS

SUPPLEMENTAL INFORMATION

Supplemental information can be found online at <https://doi.org/10.1016/j.celrep.2024.115103>.

Received: August 28, 2024

Revised: November 19, 2024

Accepted: December 3, 2024

Published: December 30, 2024; corrected online October 22, 2025

REFERENCES

1. Nigg, E.A., and Holland, A.J. (2018). Once and only once: mechanisms of centriole duplication and their deregulation in disease. *Nat. Rev. Mol. Cell Biol.* 19, 297–312. <https://doi.org/10.1038/nrm.2017.127>.
2. Al Jord, A., Lemaitre, A.-I., Delgehyr, N., Faucourt, M., Spassky, N., and Meunier, A. (2014). Centriole amplification by mother and daughter centrioles differs in multiciliated cells. *Nature* 516, 104–107. <https://doi.org/10.1038/nature13770>.
3. Al Jord, A., Shihavuddin, A., Servignat d'Aout, R., Faucourt, M., Genovesio, A., Karaïskou, A., Sobczak-Thépot, J., Spassky, N., and Meunier, A. (2017). Calibrated mitotic oscillator drives motile ciliogenesis. *Science* 358, 803–806. <https://doi.org/10.1126/science.aan8311>.
4. Vladar, E.K., Stratton, M.B., Saal, M.L., Salazar-De Simone, G., Wang, X., Wolgemuth, D., Stearns, T., and Axelrod, J.D. (2018). Cyclin-dependent kinase control of motile ciliogenesis. *Elife* 7, e36375. <https://doi.org/10.7554/elife.36375>.
5. Kim, S., Chien, Y.-H., Ryan, A., and Kintner, C. (2022). Emi2 enables centriole amplification during multiciliated cell differentiation. *Sci. Adv.* 8, eabm7538. <https://doi.org/10.1126/sciadv.abm7538>.
6. Revinski, D.R., Zaragozi, L.-E., Boutin, C., Ruiz-Garcia, S., Deprez, M., Thomé, V., Rosnet, O., Gay, A.-S., Mercey, O., Paquet, A., et al. (2018). CDC20B is required for deuterosome-mediated centriole production in multiciliated cells. *Nat. Commun.* 9, 4668. <https://doi.org/10.1038/s41467-018-06768-z>.
7. Tan, F.E., Vladar, E.K., Ma, L., Fuentealba, L.C., Hoh, R., Espinoza, F.H., Axelrod, J.D., Alvarez-Buylla, A., Stearns, T., Kintner, C., and Krasnow, M.A. (2013). Myb promotes centriole amplification and later steps of the multiciliogenesis program. *Development* 140, 4277–4286. <https://doi.org/10.1242/dev.094102>.
8. Wang, L., Fu, C., Fan, H., Du, T., Dong, M., Chen, Y., Jin, Y., Zhou, Y., Deng, M., Gu, A., et al. (2013). miR-34b regulates multiciliogenesis during organ formation in zebrafish. *Development* 140, 2755–2764. <https://doi.org/10.1242/dev.092825>.
9. Damaa, M.K., Serizay, J., Balagué, R., Boudjema, A.-R., Faucourt, M., Delgehyr, N., Goh, K.J., Lu, H., Tan, E.K., James, C.T., et al. (2024). Cyclin O controls entry into the cell-cycle variant required for multiciliated cell differentiation. *Cell Rep.* 44, 115117.
10. Choksi, S.P., Byrnes, L.E., Konjikusic, M.J., Tsai, B.W.H., Deleon, R., Lu, Q., Westlake, C.J., and Reiter, J.F. (2024). An alternative cell cycle coordinates multiciliated cell differentiation. *Nature* 630, 214–221. <https://doi.org/10.1038/s41586-024-07476-z>.
11. O'Connor, S.A., Feldman, H.M., Arora, S., Hoellerbauer, P., Toledo, C.M., Corrin, P., Carter, L., Kufeld, M., Bolouri, H., Basom, R., et al. (2021). Neural G0: a quiescent-like state found in neuroepithelial-derived cells and glioma. *Mol. Syst. Biol.* 17, e9522. <https://doi.org/10.1525/msb.20209522>.
12. La Manno, G., Siletti, K., Furlan, A., Gyllborg, D., Vinsland, E., Mossi Albiach, A., Mattsson Langseth, C., Khven, I., Lederer, A.R., Dratva, L.M., et al. (2021). Molecular architecture of the developing mouse brain. *Nature* 596, 92–96. <https://doi.org/10.1038/s41586-021-03775-x>.
13. Ruiz García, S., Deprez, M., Lebrigand, K., Cavard, A., Paquet, A., Arguel, M.-J., Magnone, V., Truchi, M., Caballero, I., Leroy, S., et al. (2019). Novel dynamics of human mucociliary differentiation revealed by single-cell RNA sequencing of nasal epithelial cultures. *Development* 146, dev177428. <https://doi.org/10.1242/dev.177428>.
14. Giotti, B., Chen, S.-H., Barnett, M.W., Regan, T., Ly, T., Wiemann, S., Hume, D.A., and Freeman, T.C. (2019). Assembly of a parts list of the human mitotic cell cycle machinery. *J. Mol. Cell Biol.* 11, 703–718. <https://doi.org/10.1093/jmcb/mjy063>.
15. Karlsson, J., Kroneis, T., Jonasson, E., Larsson, E., and Ståhlberg, A. (2017). Transcriptomic Characterization of the Human Cell Cycle in Individual Unsynchronized Cells. *J. Mol. Biol.* 429, 3909–3924. <https://doi.org/10.1016/j.jmb.2017.10.011>.
16. Schwabe, D., Formichetti, S., Junker, J.P., Falcke, M., and Rajewsky, N. (2020). The transcriptome dynamics of single cells during the cell cycle. *Mol. Syst. Biol.* 16, e9946. <https://doi.org/10.1525/msb.20209946>.
17. Zinovyev, A., Sadovsky, M., Calzone, L., Fouché, A., Groeneweld, C.S., Chervov, A., Barillot, E., and Gorban, A.N. (2021). Modeling progression of single cell populations through the cell cycle as a sequence of

- switches. *Front. Mol. Biosci.* 8, 793912. <https://doi.org/10.3389/fmolb.2021.793912>.
18. Bergen, V., Lange, M., Peidli, S., Wolf, F.A., and Theis, F.J. (2020). Generalizing RNA velocity to transient cell states through dynamical modeling. *Nat. Biotechnol.* 38, 1408–1414. <https://doi.org/10.1038/s41587-020-0591-3>.
 19. Morgan, D.O. (2007). *The Cell Cycle: Principles of Control* (New Science Press in association with Oxford University Press).
 20. Wallmeier, J., Al-Mutairi, D.A., Chen, C.-T., Loges, N.T., Pennekamp, P., Menchen, T., Ma, L., Shamseldin, H.E., Olbrich, H., Dougherty, G.W., et al. (2014). Mutations in CCNO result in congenital mucociliary clearance disorder with reduced generation of multiple motile cilia. *Nat. Genet.* 46, 646–651. <https://doi.org/10.1038/ng.2961>.
 21. Funk, M.C., Bera, A.N., Menchen, T., Kuales, G., Thriene, K., Lienkamp, S.S., Dengjel, J., Omran, H., Frank, M., and Arnold, S.J. (2015). Cyclin O (Ccno) functions during deuterosome-mediated centriole amplification of multiciliated cells. *EMBO J.* 34, 1078–1089. <https://doi.org/10.15252/embj.201490805>.
 22. Sikkema, L., Ramírez-Suástequi, C., Strobl, D.C., Gillett, T.E., Zappia, L., Madisoosn, E., Markov, N.S., Zaragoza, L.-E., Ji, Y., Ansari, M., et al. (2023). An integrated cell atlas of the lung in health and disease. *Nat. Med.* 29, 1563–1577. <https://doi.org/10.1038/s41591-023-02327-2>.
 23. Cho, R.J., Huang, M., Campbell, M.J., Dong, H., Steinmetz, L., Sapino, L., Hampton, G., Elledge, S.J., Davis, R.W., and Lockhart, D.J. (2001). Transcriptional regulation and function during the human cell cycle. *Nat. Genet.* 27, 48–54. <https://doi.org/10.1038/83751>.
 24. Whitfield, M.L., Sherlock, G., Saldanha, A.J., Murray, J.I., Ball, C.A., Alexander, K.E., Matese, J.C., Perou, C.M., Hurt, M.M., Brown, P.O., and Botstein, D. (2002). Identification of genes periodically expressed in the human cell cycle and their expression in tumors. *Mol. Biol. Cell* 13, 1977–2000. <https://doi.org/10.1091/mbc.02-02-0030>.
 25. Guo, J., Grow, E.J., Mlcochova, H., Maher, G.J., Lindskog, C., Nie, X., Guo, Y., Takei, Y., Yun, J., Cai, L., et al. (2018). The adult human testis transcriptional cell atlas. *Cell Res.* 28, 1141–1157. <https://doi.org/10.1038/s41422-018-0099-2>.
 26. Reimann, J.D., Freed, E., Hsu, J.Y., Kramer, E.R., Peters, J.M., and Jackson, P.K. (2001). Emi1 is a mitotic regulator that interacts with Cdc20 and inhibits the anaphase promoting complex. *Cell* 105, 645–655. [https://doi.org/10.1016/s0092-8674\(01\)00361-0](https://doi.org/10.1016/s0092-8674(01)00361-0).
 27. Hsu, J.Y., Reimann, J.D.R., Sørensen, C.S., Lukas, J., and Jackson, P.K. (2002). E2F-dependent accumulation of hEmi1 regulates S phase entry by inhibiting APC(Cdh1). *Nat. Cell Biol.* 4, 358–366. <https://doi.org/10.1038/ncb785>.
 28. Di Fiore, B., and Pines, J. (2007). Emi1 is needed to couple DNA replication with mitosis but does not regulate activation of the mitotic APC/C. *J. Cell Biol.* 177, 425–437. <https://doi.org/10.1083/jcb.200611166>.
 29. Pagano, M., Pepperkok, R., Verde, F., Ansorge, W., and Draetta, G. (1992). Cyclin A is required at two points in the human cell cycle. *EMBO J.* 11, 961–971. <https://doi.org/10.1002/j.1460-2075.1992.tb05135.x>.
 30. Gudas, J.M., Payton, M., Thukral, S., Chen, E., Bass, M., Robinson, M.O., and Coats, S. (1999). Cyclin E2, a novel G1 cyclin that binds Cdk2 and is aberrantly expressed in human cancers. *Mol. Cell Biol.* 19, 612–622. <https://doi.org/10.1128/MCB.19.1.612>.
 31. Scelfo, A., Angrisani, A., Grillo, M., Barnes, B.M., Muyas, F., Sauer, C.M., Leung, C.W.B., Dumont, M., Grison, M., Mazaud, D., et al. (2024). Specialized replication mechanisms maintain genome stability at human centromeres. *Mol. Cell* 84, 1003–1020.e10. <https://doi.org/10.1016/j.molcel.2024.01.018>.
 32. Chan, K.Y., Yan, C.-C.S., Roan, H.-Y., Hsu, S.-C., Tseng, T.-L., Hsiao, C.-D., Hsu, C.-P., and Chen, C.-H. (2022). Skin cells undergo asynthetic fission to expand body surfaces in zebrafish. *Nature* 605, 119–125. <https://doi.org/10.1038/s41586-022-04641-0>.
 33. Edgar, B.A., Zielke, N., and Gutierrez, C. (2014). Endocycles: a recurrent evolutionary innovation for post-mitotic cell growth. *Nat. Rev. Mol. Cell Biol.* 15, 197–210. <https://doi.org/10.1038/nrm3756>.
 34. Basu, S., Greenwood, J., Jones, A.W., and Nurse, P. (2022). Core control principles of the eukaryotic cell cycle. *Nature* 607, 381–386. <https://doi.org/10.1038/s41586-022-04798-8>.
 35. Coudreuse, D., and Nurse, P. (2010). Driving the cell cycle with a minimal CDK control network. *Nature* 468, 1074–1079. <https://doi.org/10.1038/nature09543>.
 36. McCleland, M.L., Farrell, J.A., and O'Farrell, P.H. (2009). Influence of cyclin type and dose on mitotic entry and progression in the early *Drosophila* embryo. *J. Cell Biol.* 184, 639–646. <https://doi.org/10.1083/jcb.200810012>.
 37. Royou, A., McCusker, D., Kellogg, D.R., and Sullivan, W. (2008). Grapes(Chk1) prevents nuclear CDK1 activation by delaying cyclin B nuclear accumulation. *J. Cell Biol.* 183, 63–75. <https://doi.org/10.1083/jcb.200801153>.
 38. McCleland, M.L., and O'Farrell, P.H. (2008). RNAi of mitotic cyclins in *Drosophila* uncouples the nuclear and centrosome cycle. *Curr. Biol.* 18, 245–254. <https://doi.org/10.1016/j.cub.2008.01.041>.
 39. Gavet, O., and Pines, J. (2010). Activation of cyclin B1-Cdk1 synchronizes events in the nucleus and the cytoplasm at mitosis. *J. Cell Biol.* 189, 247–259. <https://doi.org/10.1083/jcb.200909144>.
 40. Ma, J.-Y., Ou-Yang, Y.-C., Luo, Y.-B., Wang, Z.-B., Hou, Y., Han, Z.-M., Liu, Z., Schatten, H., and Sun, Q.-Y. (2013). Cyclin O regulates germinal vesicle breakdown in mouse oocytes. *Biol. Reprod.* 88, 110. <https://doi.org/10.1095/biolreprod.112.103374>.
 41. Gopinathan, L., Szmyd, R., Low, D., Diril, M.K., Chang, H.-Y., Coppola, V., Liu, K., Tessarollo, L., Guccione, E., van Pelt, A.M.M., and Kaldis, P. (2017). Emi2 Is Essential for Mouse Spermatogenesis. *Cell Rep.* 20, 697–708. <https://doi.org/10.1016/j.celrep.2017.06.033>.
 42. Liu, D., Matzuk, M.M., Sung, W.K., Guo, Q., Wang, P., and Wolgemuth, D.J. (1998). Cyclin A1 is required for meiosis in the male mouse. *Nat. Genet.* 20, 377–380. <https://doi.org/10.1038/3855>.
 43. Fernández Figueras, M.T., Alzogiby-Abi Chaker, J., Fernandez-Parrado, M., García Herrera, A., Garrido, M., Idoate Gastearena, M.Á., Llamas-Velasco, M., Monteagudo, C., Onrubia, J., Pérez Muñoz, N., et al. (2024). Principales tipos de quistes en dermatopatología: Parte 2. Rev. Española Patol. 57, 97–110. <https://doi.org/10.1016/j.patol.2023.11.007>.
 44. Rubio, C.A., Nesi, G., Zampi, G.C., de Ruiz, P.A., Jessurun, J., Jónasson, J., Hojman, R., Kogan, Z., Antonioli, D., Miller, M.L., et al. (2005). Gastric ciliated metaplasia. A study of 3406 gastrectomy specimens from dwellers of the Atlantic and the Pacific basins. *J. Clin. Pathol.* 58, 605–610. <https://doi.org/10.1136/jcp.2004.021865>.
 45. Hughes, D.L., Tsakok, M., Patel, N., Rendek, A., Bungay, H., and Silva, M.A. (2023). Ciliated Hepatic Foregut Cysts: Not as Rare as Previously Believed. *Int. J. Surg. Pathol.* 31, 260–267. <https://doi.org/10.1177/10668969221095263>.
 46. Fabien-Dupuis, C., Cooper, B., Upperman, J., Zhou, S., and Shillingford, N. (2016). Mullerian-Type Ciliated Cyst of the Thigh with PAX-8 and WT1 Positivity: A Case Report and Review of the Literature. *Case Rep. Med.* 2016, 2487820. <https://doi.org/10.1155/2016/2487820>.
 47. Spassky, N., and Meunier, A. (2017). The development and functions of multiciliated epithelia. *Nat. Rev. Mol. Cell Biol.* 18, 423–436. <https://doi.org/10.1038/nrm.2017.21>.
 48. Eymael, J., Willemse, B., Xu, J., Mooren, F., Steenbergen, E., Wetzel, J.F., Dijkman, H., Jansen, J., Van der Vlag, J., and Smeets, B. (2022). Motile Cilia on Kidney Proximal Tubular Epithelial Cells Are Associated With Tubular Injury and Interstitial Fibrosis. *Front. Cell Dev. Biol.* 10, 765887. <https://doi.org/10.3389/fcell.2022.765887>.
 49. Higginbotham, H., Bielas, S., Tanaka, T., and Gleeson, J.G. (2004). Transgenic mouse line with green-fluorescent protein-labeled Centrin 2 allows visualization of the centrosome in living cells. *Transgenic Res.* 13, 155–164. <https://doi.org/10.1023/b:trag.0000026071.41735.8e>.

50. Schindelin, J., Rueden, C.T., Hiner, M.C., and Eliceiri, K.W. (2015). The ImageJ ecosystem: An open platform for biomedical image analysis. *Mol. Reprod. Dev.* 82, 518–529. <https://doi.org/10.1002/mrd.22489>.
51. Gentleman, R.C., Carey, V.J., Bates, D.M., Bolstad, B., Dettling, M., Dudoit, S., Ellis, B., Gautier, L., Ge, Y., Gentry, J., et al. (2004). Bioconductor: open software development for computational biology and bioinformatics. *Genome Biol.* 5, R80. <https://doi.org/10.1186/gb-2004-5-10-r80>.
52. Zheng, G.X.Y., Terry, J.M., Belgrader, P., Ryvkin, P., Bent, Z.W., Wilson, R., Ziraldo, S.B., Wheeler, T.D., McDermott, G.P., Zhu, J., et al. (2017). Massively parallel digital transcriptional profiling of single cells. *Nat. Commun.* 8, 14049. <https://doi.org/10.1038/ncomms14049>.
53. Lun, A.T.L., Riesenfeld, S., Andrews, T., Dao, T.P., Gomes, T., and participants in the 1st Human Cell Atlas Jamboree; and Marioni, J.C. (2019). EmptyDrops: distinguishing cells from empty droplets in droplet-based single-cell RNA sequencing data. *Genome Biol.* 20, 63. <https://doi.org/10.1186/s13059-019-1662-y>.
54. Haghverdi, L., Lun, A.T.L., Morgan, M.D., and Marioni, J.C. (2018). Batch effects in single-cell RNA-seq data are corrected by matching mutual nearest neighbors. *Nat. Biotechnol.* 36, 421–427. <https://doi.org/10.1038/nbt.4091>.
55. Lun, A.T.L., McCarthy, D.J., and Marioni, J.C. (2016). A step-by-step workflow for low-level analysis of single-cell RNA-seq data with Bioconductor. *F1000Res.* 5, 2122. <https://doi.org/10.12688/f1000research.9501.2>.
56. McCarthy, D.J., Campbell, K.R., Lun, A.T.L., and Wills, Q.F. (2017). Scater: pre-processing, quality control, normalization and visualization of single-cell RNA-seq data in R. *Bioinformatics* 33, 1179–1186. <https://doi.org/10.1093/bioinformatics/btw777>.
57. Aran, D., Looney, A.P., Liu, L., Wu, E., Fong, V., Hsu, A., Chak, S., Naikawadi, R.P., Wolters, P.J., Abate, A.R., et al. (2019). Reference-based analysis of lung single-cell sequencing reveals a transitional profibrotic macrophage. *Nat. Immunol.* 20, 163–172. <https://doi.org/10.1038/s41590-018-0276-y>.
58. Street, K., Risso, D., Fletcher, R.B., Das, D., Ngai, J., Yosef, N., Purdom, E., and Dudoit, S. (2018). Slingshot: cell lineage and pseudotime inference for single-cell transcriptomics. *BMC Genom.* 19, 477. <https://doi.org/10.1186/s12864-018-4772-0>.
59. Kolberg, L., Raudvere, U., Kuzmin, I., Vilo, J., and Peterson, H. (2020). gprofiler2 – an R package for gene list functional enrichment analysis and namespace conversion toolset g:Profiler. *F1000Res.* 9, ELIXIR-709. <https://doi.org/10.12688/f1000research.24956.2>.
60. Hao, Y., Stuart, T., Kowalski, M.H., Choudhary, S., Hoffman, P., Hartman, A., Srivastava, A., Molla, G., Madad, S., Fernandez-Granda, C., and Satija, R. (2024). Dictionary learning for integrative, multimodal and scalable single-cell analysis. *Nat. Biotechnol.* 42, 293–304. <https://doi.org/10.1038/s41587-023-01767-y>.
61. Van den Berge, K., Roux de Bézieux, H., Street, K., Saelens, W., Cannoodt, R., Saeys, Y., Dudoit, S., and Clement, L. (2020). Trajectory-based differential expression analysis for single-cell sequencing data. *Nat. Commun.* 11, 1201. <https://doi.org/10.1038/s41467-020-14766-3>.
62. Wickham, H., Averick, M., Bryan, J., Chang, W., McGowan, L., François, R., Grolemund, G., Hayes, A., Henry, L., Hester, J., et al. (2019). Welcome to the Tidyverse. *J. Open Source Softw.* 4, 1686. <https://doi.org/10.21105/joss.01686>.

STAR★METHODS

KEY RESOURCES TABLE

REAGENT or RESOURCE	SOURCE	IDENTIFIER
Antibodies		
Mouse IgG2b Anti-Actin Antibody (C4)	Millipore	Cat# MAB1501; RRID:AB_2223041
Rat Anti-tyrosinated tubulin (YL1/2)	Abcam	Cat# ab6160; RRID:AB_305328
Mouse IgG1 Anti-Nuclear Pore Complex Proteins Monoclonal Antibody (Mab414)	Eurogentec	Cat# MMS-120P-100; RRID:AB_291294
Rabbit Anti-HA Antibody	Cell Signaling	Cat# 3724; RRID:AB_1549585
Mouse IgG1 Monoclonal Anti Polyglutamylation Modification (GT335)	AdipoGen	Cat# AG-20B-0020, Clone GT335; RRID: AB_2490210
Mouse IgG2b Monoclonal Anti FOP	Abnova Corporation	Cat# H00011116-M01; Clone: 2B1; RRID: AB_463883
Rabbit Anti Histone 3 Serine 10 P	Cell Signaling	Cat# 9701; RRID:AB_331535
Bacterial and virus strains		
pAV[Exp]-CMV>EGFP	VectorBuilder	VB010000-9299hac
pAV[Exp]-CMV>Myc/mFbxo5	VectorBuilder	VB220220-1057frt
pAV[Exp]-CMV>HA/mCcna2	VectorBuilder	VB220220-1059gxr
pAV[Exp]-mCherry-CMV>HA/mCcne2	VectorBuilder	VB230105-1113bjk
Chemicals, peptides, and recombinant proteins		
PD 166285 dihydrochloride	Tocris Bioscience	Cat# 37852; Pubchem# 9916391
EdU (5-ethynyl-2-deoxyuridine)	Thermo Fisher Scientific	Cat# 11590926; CAS: 61135-33-9
Critical commercial assays		
Click-iT® EdU Imaging Kit	ThermoFisher	C10337
Single Cell 3' kit	10X Genomics	Chemistry v3.1
Deposited data		
Raw and analyzed scRNAseq data	This paper	GEO: GSE201773; https://cellxgene.cziscience.com/collections/33f48a52-31d8-4cc8-bd00-1e89c659a87f
Original code for this study	This paper	https://doi.org/10.5281/zenodo.14105247
Single-cell RNA-seq data of human adult spermatogenesis	Guo et al. ²⁵	GEO: GSE112013
An integrated cell atlas of the human lung in health and disease (core)	Sikkema et al. ²²	Cellxgene collection: 6f6d381a-7701-4781-935c-db10d30de293
Single-cell RNA-seq dataset of the human airway epithelial cells in air-liquid interface (ALI) culture for 28 days	Ruiz-Garcia et al. ¹³	GEO: GSM3439922
Single-cell RNA-seq data of mouse tracheal embryonic cells in air-liquid interface (ALI) culture for 3 days	Ruiz-Garcia et al. ¹³	GEO: GSM3439924
In vivo single-cell RNA-seq data of the brain during mouse embryonic development	La Manno et al. ¹²	https://storage.googleapis.com/linnarsson-lab-loom/dev_all.loom
Experimental models: Organisms/strains		
C57Bl/6J	Gift from the laboratory of Gabriel Gil-Gomez	N/A
C57Bl/6N	Gift from the laboratory of Andrew Holland	N/A
RjORL:SWISS	Janvier Labs	N/A
Cen2-GFP: CB6-Tg(CAG-EGFP/CETN2) 3-4Jgg/J	The Jackson Laboratory ⁴⁹	Cat# JAX:008234; RRID: IMSR_JAX:008234

(Continued on next page)

Continued

REAGENT or RESOURCE	SOURCE	IDENTIFIER
Software and algorithms		
ImageJ	Schindelin et al. ⁵⁰	https://imagej.nih.gov/ij/download.html ; RRID: SCR_003070
R v4.4.1	R-project	https://www.r-project.org/
Bioconductor v3.19	Gentleman et al. ⁵¹	https://www.bioconductor.org/
10x Genomics Cell Ranger v5.0.1	Zheng et al. ⁵²	https://www.10xgenomics.com/support/software/cell-ranger/latest
DropletUtils 1.24.0	Lun et al. ⁵³	https://www.bioconductor.org/
batchelor 1.20.0	Haghverdi et al. ⁵⁴	https://www.bioconductor.org/
scran 1.32.0	Lun et al. ⁵⁵	https://www.bioconductor.org/
scater 1.32.0	McCarthy et al. ⁵⁶	https://www.bioconductor.org/
scuttle 1.14.0	McCarthy et al. ⁵⁶	https://www.bioconductor.org/
igraph 2.0.3	Csardi et al.	https://cran.r-project.org/web/packages/igraph/index.html
SingleR 2.6.0	Aran et al. ⁵⁷	https://www.bioconductor.org/
slingshot 2.12.0	Street et al. ⁵⁸	https://www.bioconductor.org/
gprofiler2 0.2.3	Kolberg et al. ⁵⁹	https://cran.r-project.org/web/packages/gprofiler2/index.html
Seurat 5.1.0	Hao et al. ⁶⁰	https://cran.r-project.org/web/packages/Seurat/index.html
tradeSeq 1.18.0	Van den Berg et al. ⁶¹	https://www.bioconductor.org/
scvelo 0.2.5	Bergen et al. ¹⁸	https://scvelo.readthedocs.io/en/stable/
ggplot2 3.5.1	Whickam ⁶²	https://cran.r-project.org/web/packages/ggplot2/index.html
tidyverse 2.0.0	Whickam ⁶²	https://cran.r-project.org/web/packages/tidyverse/index.html

EXPERIMENTAL MODEL AND STUDY PARTICIPANT DETAILS

Animals

All animal studies were performed in accordance with the guidelines of the European Community and French Ministry of Agriculture and were approved by the “Direction départementale de la protection des populations de Paris” (Approval number Ce5/2012/107; APAFiS #9343). The mouse strains used for scRNAseq profiling are C57Bl6J or C57Bl6N, and the strains used for immunofluorescence stainings are RjOrl:SWISS (Janvier labs) or a Cen2-GFP transgenic line, obtained from the Jackson Laboratory (JAX:008234).⁵¹ Both Cen2-GFP^{+/−} and Cen2-GFP^{−/−} pups were used for the study since no differences between the two have been reported.

METHOD DETAILS

Single-cell RNA-seq of *in vitro* differentiating multiciliated cells

Newborn mice (C57Bl6N or C57Bl6J, P0-P2) were sacrificed by decapitation. The brains were then dissected in Hank’s solution (10% HBSS, 5% HEPES, 5% sodium bicarbonate, 1% penicillin/streptomycin (P/S) in pure water) and the extracted ventricular walls were cut manually into pieces, followed by enzymatic digestion (DMEM glutamax, 33% papain (Worthington 3126), 17% DNase at 10 mg/mL, 42% cysteine at 12 mg/mL) for 45 min at 37°C in a humidified 5% CO₂ incubator. Digestion was stopped by addition of a solution of trypsin inhibitors (Leibovitz Medium L15, 10% ovomucoid at 1 mg/mL, 2% DNase at 10 mg/mL). The cells were then washed in L15 and resuspended in DMEM glutamax supplemented with 10% fetal bovine serum (FBS) and 1% P/S in a Poly-L-lysine (PLL)-coated flask (equivalent of 2 ventricular walls per 25cm² flask). Ependymal progenitors proliferated for 4–5 days until confluence, followed by shaking (250rpm) overnight to remove contaminant cells (neurons, oligodendrocytes, etc.). The day after shaking, the flasks’ medium was changed to warm serum-free DMEM glutamax 1% P/S to trigger ependymal cell differentiation for 2 days. At this time point, cells at all stages of cell cycle or ependymal differentiation are present in the flask. After 2 days of *in vitro* differentiation, flasks were rinsed with PBS 1X twice and treated by enzymatic cell dissociation (Trypsin, 1mL) for 10 min and trituration to obtain a single cell suspension. Digestion was stopped by addition of 1 mL of fetal bovine serum (FBS). The cells were then washed in serum-free DMEM glutamax 1% P/S and resuspended in HBSS-0.1% BSA for single-cell RNA-seq library preparation. Cell cultures from three different animals with the same genetic background and treatment were pooled together; to multiplex them, samples were

labeled using a cell surface protein labeling strategy following manufacturer's instructions (https://assets.ctfassets.net/an68im79xiti/5KA1NbZdTOam8A0yq6KyC2/f3e0479ff7b1c1633e6ddf8959a88a3b/CG000149_DemonstratedProtocol_CellSurfaceProteinLabeling_Rev_A.pdf), using TotalSeq hashtag antibodies (BioLegend). However, the efficiency of the cell hashing did not allow to unambiguously separate cells coming from different animals and was therefore not used in downstream analysis. Cell suspensions were passed through a 40 µm Flowmi cell strainer (BelArt) and cell concentrations were carefully evaluated with a Countess FL automated cell counter (Thermofisher). For single cell RNA-seq, cells were partitioned with a Chromium equipment (10X Genomics) and libraries were prepared using the standard Single Cell 3' v3.1 protocol (10X Genomics). Sequencing was performed on an Illumina NextSeq 500 sequencing machine following manufacturer's instructions, on a high Flowcell, using the following sequencing cycles: 28b for read 1, 55b for read 2, 8b for index.

Adenovirus infections

The following adenovirus gene expression systems were ordered and packaged by VectorBuilder: pAV[Exp]-CMV>EGFP (control eGFP), pAV[Exp]-CMV>Myc/mFbxo5 (EMI1, tagged with myc in N-terminal, under the control of CMV), pAV[Exp]-mCherry-CMV>HA/mCcne2 and pAV[Exp]-mCherry-CMV>HA/mCcna2 (CCNE2 or CCNA2, tagged with HA in N-terminal, under the control of CMV in a vector also expressing mCherry). Mouse F box5 (Emi1) mRNA (NM_025995.2), Ccne2 mRNA (NM_001037134.2) and Ccna2 mRNA (NM_009828.3) references were used.

For adenovirus infections, ependymal cell cultures were performed as described above, although cells were plated on Poly-L-lysine (PLL)-coated 12mm coverslips in 24-well plates after tissue dissociation. After 2 days of *in vitro* differentiation (DIV2), adenovirus infections were performed by adding the adenovirus crude lysates to differentiating multiciliated progenitors (500 MOI for single infections, 500 MOI each for co-infection with 2 viruses) for 4h, shaking every hour for optimal infection. Cells were washed with pre-warmed 0.5% FBS-DMEM, and infected cells were kept in culture for 20h or 92h under serum-starved condition with 0% FBS-DMEM. The cells were then fixed and subjected to analysis according to days post infection (DPI).

Immunostainings and EdU incorporation stainings

EdU was added after 4h of viral infection, immediately after virus wash-out. Cell cultures were fixed 24h or 96h post-infection (20h or 90h EdU incorporation) in paraformaldehyde (PFA 4%) at 4°C for 10 min, then pre-blocked in saturation buffer (PBS 1X with 0.2% Triton X-100 and 10% FBS). Primary antibody immunostaining was performed for 1h at room temperature in the saturation buffer. When needed, EdU incorporation was labeled using the ThermoFisher Click-iT EdU Imaging Kit (catalog #C10337) following manufacturer's recommendations. Cells were then washed in PBS and secondary antibody staining performed for 1h at room temperature in the saturation buffer. Cells were mounted in DAPI Fluoromount (Southern Biotech). The following antibodies were used: Rabbit anti-Histone 3 (pSer10; 1:100; 9701, Cell Signaling), Mouse IgG2b Monoclonal Anti FOP (1:700; 2B1, Abnova Corporation), Mouse IgG1 Monoclonal Anti Polyglutamylated Modification (GT335) (1:700; AG-20B-0020, AdipoGen), Rabbit Anti-HA Antibody (1:400; 3724, Cell Signaling), Mouse IgG1 Anti-Nuclear Pore Complex Proteins Monoclonal Antibody (Mab414) (1:2500; MMS-120P-100, Eurogentec), Rat Anti-tyrosinated tubulin (YL1/2) (1:200; ab6160, Abcam), Mouse IgG2b Anti-Actin Antibody (C4) (1:200; MAB1501; Millipore), and species-specific Alexa Fluor secondary antibodies (1:400; Invitrogen).

Computational analyses

Pre-processing of scRNAseq of *in vitro* differentiating multiciliated cells

Fastq file demultiplexing, barcode processing, gene counting, and aggregation were made using the Cell Ranger software following 10X Genomics guidelines. 10X Genomics mm10 genome reference and gene annotations compiled in 2020 were used (https://support.10xgenomics.com/single-cell-gene-expression/software/release-notes/build#mm10_2020A). Empty cells (detected by emptyDrops from DropletUtils) were filtered out and only protein-coding genes were retained.

Batch correction, dimensionality reduction, clustering

Batch correction and replicate merging was performed using fast MNN correction from batchelor package, using only marker genes identified in either one of the replicates using scran package. For visualization, UMAP embedding was performed using 50 dimensions from the corrected PCA; the embedding was performed several times with a changing seed and a representative 2D projection of the dataset was used. Cell clustering was performed on the dataset embedded in an SNN graph (k = 5 neighbors), using the Louvain algorithm from igraph.

Cell annotation

Clusters were manually annotated using cell markers identified in previous studies, and annotations were validated using automated annotation transfer (relying on SingleR package) from a reference collection of 358 bulk RNA-seq profiles of sorted cell populations.

Gene annotation

Genes in any given cell cluster were annotated as expressed as long as they had a log-normalized expression greater than 0.5 in more than 20% of the cells within the cell cluster. Genes differentially expressed between cell populations were identified using the "findMarkers" function from the scran package. Any gene with an expression fold-change greater than 1.5 between two cell clusters was considered enriched in the cluster with the greatest expression.

Cluster stability

Cluster stability was estimated by clustering 80% randomly sampled cells from the original dataset 30 times independently and comparing the clustering of each cell to the original clustering.

Cell cycle phase annotation

Putative cell cycle phases were transferred from a recent scRNAseq dataset of proliferating neural stem cells with annotated cell cycle phases (O'Connor et al., 2021,¹¹) using SingleR. G0, G1 and Late G1 labels were collapsed to a single “G1” label.

Trajectory analysis

Trajectory and pseudotime inferences were performed using PCA embedded data with slingshot, specifying start (proliferating progenitors) and end clusters (terminally differentiated MCCs) to orientate the trajectory. Computed pseudotime was scaled between 0 and 1 for clarity. Continuous gene expression along the slingshot-inferred trajectory was modeled using a generalized additive model. For visualization of the continuous expression of many variable genes along the slingshot-inferred trajectory (e.g., in Figure S2C), genes were first clustered using k-medoids then seriated using the spectral method from the seriation package.

GO enrichment analysis

GO over-representation analysis was conducted for individual gene sets using the gprofiler2 package.

Combined analysis of cycling progenitors and deuterosomal cells

Combined sub-processing of both cycling progenitor cells and all the deuterosomal cells was done by performing batch correction and replicate merging on the aggregated subsets of cells, using a large set of cell cycle-related genes obtained from GO mouse annotation database. For visualization, UMAP embedding was performed using 50 dimensions from the corrected PCA; the embedding was performed several times with a changing seed and a representative 2D projection of the dataset was used. Cell sub-clustering was performed using the same strategy as that used in the complete dataset (see hereinabove). The number of nearest cycling progenitor (deuterosomal) neighbors for deuterosomal cells (progenitors) (from zero to five) was calculated within the five nearest neighbors identified using Euclidean distance between pairs of cells embedded in corrected PCA space. This was performed either on the real cycling progenitors and deuterosomal merged dataset, or on a dataset containing real cycling progenitor cells and simulated uncorrelated cells, using the splatter package.

Identification of angular progression of cycling and deuterosomal cells: Independent sub-processing of either the cycling progenitor cells ($n = 759$) or all the deuterosomal cells ($n = 2911$) was done by performing batch correction and replicate merging on each cell subset, using the cell cycle-annotated genes or the combined oscillatory and transiently expressed gene sets, respectively. The circular cell trajectories in the resulting corrected PCA embedding, depicted as a black line in Figure 3, were computed for each subset of cells using a smoothed spline passing by the center of mass of each of twelve angular bins equally distributed around the origin of the two first PCA dimensions. The angular progression of each cell along this circular cell trajectory, bound between 0 and 2π , was then defined as the angle between the origin placed at (0, 1) and the cell itself, in the clockwise direction. These angular progression scores were shifted (modulo 2π) in order for the 0 to align with the beginning of the cell cycle for cycling progenitors or with the beginning of the early deuterosomal cell population for deuterosomal cells. Continuous gene expression along the angular progression of either cycling progenitors (“cell cycle”) or deuterosomal cells (“MCC cell cycle variant”) was modeled using a generalized additive model using the tradeSeq package. Genes with a varying expression along either progenitor or deuterosomal cell circular trajectories were identified using the associationTest from the tradeSeq package as genes with a fold-change greater than 2 and a p -value lower than 0.01.

RNA velocity analysis

RNA velocity was calculated using the “dynamic” mode from scvelo software and for visualization, the RNA velocity vector field was embedded in UMAP projection of the dataset using velociraptor package. Individual RNA velocity vectors were decomposed in normal and tangential components using a coordinate plane orthogonal to each cell’s angular progression.

Gene-cyclin correlation analysis

The pairwise Spearman correlation scores for the expression between any gene and any individual cyclin was computed. Any correlation score greater than 0.3 (with an associated p -value lower than 0.01) was then used to compute a correlation network with four nodes corresponding to each cyclin. Non-redundant sets of cyclin-coordinated genes were built by associating each gene to its most correlated cyclin.

scRNAseq analysis of mouse brain during embryonic development (in vivo)

In vivo single-cell RNA-seq data of the brain during mouse embryonic development was retrieved from La Manno et al., 2021¹² (https://storage.googleapis.com/linnarsson-lab-loom/dev_all.loom). Glial pre-annotated cells older than E16 were extracted and batch effects associated with “batch”, “replicate”, “age” and “ChipID” annotations were regressed out using regressBatches correction from batchelor package, using only marker genes identified in any of the replicates using scran package. For visualization, UMAP embedding was performed using 50 dimensions from the corrected PCA; the embedding was performed several times with a changing seed and a representative 2D projection of the dataset was used. Pre-existing cell clustering was used to re-annotate cell types and cell types irrelevant for this study (neuroblasts, oligodendrocytes, sub-commisural cells, hypendemal cells and Pdlim4+ cells) were removed. Cell re-clustering was performed on the remaining cells embedded in an SNN graph ($k = 5$ neighbors) using the Louvain algorithm from igraph, and clusters were manually annotated using MCC differentiation markers. Putative cell cycle phases were annotated using Seurat. Genes in any given cell cluster were annotated as expressed as long as they had a log-normalized expression greater than 0.5 in more than 10% of the cells within the cell cluster.

Independent sub-processing of deuterosomal cells was done by re-embedding deuterosomal cells only in a PCA dimensional space. The same approach described hereabove was then used to compute a circular cell trajectory and to model continuous gene expression along the angular progression of deuterosomal cells.

scRNAseq analysis of mouse tracheal embryonic cells (in vitro)

Single-cell RNA-seq data of mouse tracheal embryonic cells in air-liquid interface (ALI) culture for 3 days was obtained from Ruiz-Garcia et al., 2019¹³ (GEO accession ID: GSM3439924). Empty cells (detected by emptyDrops from DropletUtils) were filtered out and only protein-coding genes were retained. The dataset was embedded in a lower PCA 50-dimension space with removed technical noise, using denoisePCA function from the scuttle package. Cell clustering was performed on cells embedded in an SNN graph using the Louvain algorithm from igraph, and clusters were manually annotated using MCC differentiation markers as well as markers for other cell types commonly found in respiratory tracts. Putative cell cycle phases were annotated using Seurat. Genes in any given cell cluster were annotated as expressed as long as they had a log-normalized expression greater than 0.5 in more than 20% of the cells within the cell cluster.

scRNAseq analysis of human airway embryonic cells (in vitro)

Pre-processed data of single-cell RNA-seq dataset of the human airway epithelial cells in air-liquid interface (ALI) culture for 28 days (Ruiz-Garcia et al., 2019,¹³ GEO accession ID: GSM3439922) was provided by the authors. Only protein-coding genes were retained. Cell clusters, annotations and embeddings in PCA or t-SNE provided by the authors were used. Putative cell cycle phases were annotated using Seurat. Genes in any given cell cluster were annotated as expressed as long as they had a log-normalized expression greater than 0.5 in more than 10% of the cells within the cell cluster.

scRNAseq analysis of human airway epithelial cells (in vivo)

Pre-processed data of a 500K single-cell RNA-seq dataset of human airway epithelial cells (HLCA: Human Lung Cell Atlas) (Sikkema et al. 2023²²) was recovered from Cellxgene (<https://cellxgene.cziscience.com/collections/6f6d381a-7701-4781-935c-db10d30de293>).

1,004 pre-annotated deuterosomal cells were extracted and further processed. Putative cell cycle phases were annotated using Seurat. The same approach described hereabove was then used to compute a circular cell trajectory and to model continuous cyclin expression along the angular progression of deuterosomal cells.

scRNAseq analysis of human spermatogenesis (in vivo)

Single-cell RNA-seq data of human adult spermatogenesis was obtained from Guo et al., 2018²⁵ (GEO accession ID: GSE112013). Cell annotations were retrieved from UCSC (<https://cells.ucsc.edu/testis/meta.tsv>) and irrelevant cells (endothelial cells, Sertoli cells, macrophages) were filtered out. Only protein-coding genes were retained. Batch effects associated with “donor” annotations were removed using fastMNN correction from batchelor package, using the 10% most variable genes. For visualization, t-SNE embedding was performed using 50 dimensions from the corrected PCA; the embedding was performed several times with a changing seed and a representative 2D projection of the dataset was used. Trajectory and pseudotime inferences were performed using PCA embedded data with slingshot, specifying start and end clusters to orientate the trajectory. Continuous gene expression along the slingshot-inferred trajectory was modeled using a generalized additive model.

QUANTIFICATION AND STATISTICAL ANALYSIS

When summarizing gene expression using point-range representation (e.g., [Figure S4](#)), Each point represents the mean value of the dataset, while the range extends to represent the mean \pm two standard deviations.

When performing differential gene expression analysis (e.g., [Figures 2](#) and [S4](#)), genes differentially expressed between cell populations were identified using the “findMarkers” function from the scran package. Any gene with an expression fold-change greater than 1.5 between two cell clusters was considered enriched in the cluster with the greatest expression, and consequently was labeled with a star *.

When performing GO over-representation analysis (e.g., [Figures S3](#) and [4](#)), BH-corrected *p*-values were computed for individual gene sets using the gprofiler2 package.

When comparing proportions of cells (e.g., [Figures 5](#) and [S7](#)), the *p*-values are calculated using Fisher’s exact tests, and summarized as follows: * = *p*-value <0.05, ** = *p*-value <0.01, *** = *p*-value <0.001.

When boxplot representation is used (e.g., [Figures 5](#) and [S7](#)), each boxplot shows the median (horizontal line inside the box), the interquartile range (IQR; represented by the height of the box, spanning from the 25th to the 75th percentile), and potential outliers. The “whiskers” extend from the box to the smallest and largest values within 1.5 times the IQR from the lower and upper quartiles, respectively.

Other statistical analyses, in particular for scRNAseq investigation, are described in the relevant subsections of the “Computational analyses” subsection of the STAR Methods.